Title
Large Scale Human Activity Monitoring for Diverse Subjects

Author
Xu, Xiaoyu

Publication Date
2012

Peer reviewed|Thesis/dissertation

UNIVERSITY OF CALIFORNIA

Los Angeles

Large Scale Human Activity Monitoring for Diverse Subjects

A dissertation submitted in partial satisfaction

of the requirements for the degree

Doctor of Philosophy in Electrical Engineering

by

Xiaoyu Xu

2013

ABSTRACT OF THE DISSERTATION

Large Scale Human Activity Monitoring for Diverse Subjects

by

Xiaoyu Xu

Doctor of Philosophy in Electrical Engineering

University of California, Los Angeles, 2013

Professor William J. Kaiser, Chair

Assurance of outcome is critical for patients that are afflicted with neurological disorders (for example stroke that introduces hemiparetic gait) and motion is a critical indicator of outcome. However outcome in the community environment is very difficult to determine. Wearable sensing system, due to its low cost, energy efficient, non-intrusive and applicable for large-scale development, is feasible for remote, continuous monitoring of motion and activities and thus provide outcome measures in the community. Towards this goal, this thesis explores the following problems:

1. A precise motion classification system is introduced. It is applicable for diverse subjects whose motion ability ranges from very disabled to very capable and suitable for complicated community environment. Critical kinematic parameters of motion is modeled, characterized and validated, which provides direct outcome measures in the community. Those methods are applied to a large-scale trial with stroke patients. The problems encountered in large-scale trial and the corresponding engineering solutions are summarized.

2. For effective feedback provision, a PCA based visualization method is proposed, where gait quality evolution path is shown. It also introduces a gait quality vector

and in particular, a metric to measure uncertainty in gait.

3. The individualized motion classification model is extended into a population based analysis. First an indexing method for data dimension reduction is proposed. The indexing method expedites the processing speed and maintains least critical information loss for motion analysis. Second, hierarchical clustering method is employed to derive the primitive gait patterns from the stroke population. The developed techniques help scale the motion classification system for big data.

The dissertation of Xiaoyu Xu is approved.

Bruce Dobkin

Lieven Vandenberghe

Alex Bui

Greg Pottie

William J. Kaiser, Committee Chair

University of California, Los Angeles

2013

To my parents, my husband and my daughter.

TABLE OF CONTENTS

LIST OF FIGURES

LIST OF TABLES

ACKNOWLEDGMENTS

First and foremost, I would like to thank my advisor, Professor William Kaiser, for giving me the opportunity to conduct fascinating research in motion sensing, as well as his invaluable support and visionary guidance during my study on this particular research direction.

My gratitude also goes to my current thesis committee members: Professors Greg Pottie, Alex Bui, Lieven Vandenberghe and Bruce Dobkin. I thank doctor Bruce Dobkin for his expert guidance and support in conducting the SIRRACT study. I thank other members, for their insightful discussions, advice and help in various aspects.

I feel very fortunate to have worked with my excellent fellow group members at ASCENT lab, UCLA Wireless Health Institute and collaborators from Neurology department (in alphabetical order) Mahdi Ashktorab, Laurence Au, Maxim Batalin, Henrik Borgstrom, Victor Chen, Andrew Dorsch, Yeung Lam, Manda Paul, Digvijay Singh, Seth Thomas, Frank Wang, Yan Wang, James Xu and Eric Yuen. I have benefited greatly from their peer interactions and friendships during the past four years. I thank Maxim Batalin for his help, guidance and valuable discussion during the early years of my Ph.D. I'm always encouraged by his positive attitude.

Last, but not least, I would like to dedicate this thesis to my parents, my husband Wenze Hu and my five month old daughter Ruby Hu, for their love, patience, and understanding. They teach me to appreciate life and be grateful.

VITA

2006	B.S., Electronics and Communication Engineering, Beijing Jiaotong University
2008	M.S., Electrical Engineering, Beijing Jiaotong University
2008	B.A., Economics, Peking University
2008-2012	Graduate Student Researcher, Department of Electrical Engineering, University of California, Los Angeles

PUBLICATIONS

Andre Dorsch, Seth Thomas, **Xiaoyu Xu**, and William Kaiser. Remote Activity Monitoring Quantifies Changes in Gait During Acute Inpatient Rehabilitation. In *Wireless Health (WH), 2012*

Xiaoyu Xu, Maxim A. Batalin, Yan Wang and William J. Kaiser. Gait Quality Evaluation Method For Post-stroke Patients. *IEEE International Conference on Acoustics, Speech, and Signal Processing (ICASSP), 2012*

Yan Wang, **Xiaoyu Xu**, Maxim A. Batalin and William J. Kaiser. Detection of Upper Limb Activities using Multimode Sensor Fusion. *Biomedical Circuits and System Conference (BioCAS)*, 2011

Xiaoyu Xu, Digvijay Singh, Maxim A. Batalin and William J. Kaiser. StepFit: A Novel Fitness Evaluation System. *International Conference on Body Area Networks (BodyNets)*, 2011

Lawrence Au, Alex A. T. Bui, Maxim A. Batalin, **Xiaoyu Xu**, William J. Kaiser. CARER: Efficient Dynamic Sensing for Continuous Activity Monitoring. *Annual International Conference of the IEEE Engineering in Medicine and Biology Society (EMBC), 2011*

Xiaoyu Xu, Maxim A. Batalin, Bruce Dobkin, and William J. Kaiser. Robust Hierarchical System for Classification of Complex Human Mobility Characteristics in the Presence of Neurological Disorders. *International Conference on Body Sensor Networks (BSN)*, 2011

Bruce Dobkin, Seth Thomas, **Xiaoyu Xu**, Maxim A. Batalin, and William J. Kaiser. Reliability of bilateral ankle accelerometer algorithms for activity pattern recognition and walking speed after stroke. In *Stroke*, 2011

Lawrence K. Au, Maxim A. Batalin, Brett Jordan, **Xiaoyu Xu**, Alex A. T. Bui, Bruce Dobkin, and William J. Kaiser. Demonstration of whi-fit: a wireless- enabled cycle restorator. In *Wireless Health (WH), 2010*

CHAPTER 1

Introduction

1.1 Motivations and Objective

Continued rapid progress in cost reduction, energy efficiency, and new data transport architectures for body worn sensors enables remote monitoring of patient activity as well as fitness assessment and feedback with critical focus and impact on successful outcomes in healthcare. Monitoring systems, composed of both sensor and signal processing systems seek to provide the capability to classify subject motion state and characteristics.

Fitness advancement has been shown to be one of the most effective interventions against disease and critical to the promotion of general health and wellness. At the same time, fitness evaluation and development of appropriate intervention techniques traditionally requires participation of experienced trainers or physician and expensive equipment and dedicated instrumented exercise facilities. Furthermore, while critically important in maintenance of health, fitness evaluation is not available to most individuals due to cost and facility access. In this thesis, we also present automated low cost system for fitness evaluation and promotion.

The remote, continuous monitoring of human motions are central to healthcare for advancing neurological rehabilitation. It improves patient outcomes, facilitates patient-health provider communication and reduces cost in healthcare. Monitoring system progress has currently enabled classification of normal gait or abnormal gait within

constrained laboratory operating conditions. However, monitoring of subjects in the community (specifically in residential environments remote from the laboratory or urban outdoor environments) has introduced fundamental challenges that have not been solved in the past. These challenges become profoundly more severe when monitoring subjects suffering from impaired gait due to conditions including stroke and other neurological disorders. In this thesis, we present a couple of novel algorithms and models to solve this problem.

The following missions are aimed.

- Enable the first, accurate, validated, convenient technology for tracking human motion in the community.
- Our technology will exploit the lowest cost and most ubiquitous wearable sensor technology.
- To enable a large research community to exploit both technology and the accompanying tools, to advance the outcomes and technology.
- This research is unique as a result of both new algorithms and software system architectures, specifically optimized for wearable motion sensors.

1.2 Background I: Motion Classification And Activity Recognition System

Several motion capture and activity recognition technologies have been proposed previously.

Acoustic tracking systems use ultrasonic pulses and can determine position through time-of-flight of the pulse. The transmitter and be either placed on a body segment or fixed in the measurement volume. Sensors can be occluded and the accuracy is

vulnerable to reflection of sound [Priyantha et al., 2000; Vlasic et al., 2007].

Mechanical systems utilize rigid or flexible goniometers or exoskeletons, which are worn by the performer, to measure the joint angles directly. Those systems are uncomfortable to wear and may potentially impede the motion. The cost of the system is very high and make it hard for large-scale deployment[Met; Sha].

Magnetic systems utilize sensors placed on the body to measure magnetic fields, which is generated by three perpendicular coils that emit a magnetic filed when a current is applied. Even though human body is transparent to magnetic fields, magnetic fields decrease in power rapidly as the distance from the generating source increases and they can easily be disturbed by magnetic materials nearby [mot; Pol].

Optical motion capture system track reflective markers or light-emitting diodes placed on the body. Exact 3D marker locations are computed from the images recorded by the surrounding cameras using triangulation methods. The major disadvantages of this approach are extreme cost and lack of portability [VIC; Opt]. Image-based systems, which are markerless, use computer vision techniques to derive motion parameters from video [Aggarwal and Ryoo, 2011]. The camera-based systems are not self-contained and need cameras deployed in environment, besides both of these two methods will suffer from privacy issues and are not feasible for large-scale deployment.

Resistive sensors, such as flex sensor and pressure sensors, supplement motion capture technologies. Resistive sensors have different resistance outputs when deformed or pressed with different forces. Flex sensor measures joint angles, such as hand motion (finger flexion), elbow flexion and knee flexion [Wang et al., 2011; Gibbs and Asada, 2005]. Pressure sensor can be utilized to measure locomotion dynamics by putting within insole or mat [GAI]. Those sensors, constrained by their physical properties, only apply to specific applications.

1.3 Background II: Wearable Sensor Systems

The wearable sensor system is primarily composed of inertial sensor systems with combination of other wearable sensing system discussed in section 1.2.

The inertial sensors include accelerometers, gyroscopes, magnetometers. Accelerometer measures proper acceleration, which is the acceleration relative to a free fall; Gyroscope measures angular rate, which is the speed of rotation. Magnetometer measures magnetic field.

Motion classification using wearable sensors has drawn interests of research for over a decade. [Mathie et al., 2004] uses one trial-axial accelerometer mounted on waist to classify activities and verifies results in controlled laboratory conditions. [Roetenberg et al., 2007] and [Schepers and Veltink, 2010] combines magnetic sensors and inertial sensors and uses Kalman filter to detect body rotation and position, at a low moving rate. In [Roetenberg et al., 2009] the author further deploys a biomechanical model of joints and segments for human body by the same sensor setting. It provides a graphic reconstruction of motion. [Vlasic et al., 2007] combines acoustic signal and inertial sensors to reconstruct a variety range of motions with graphics and achieves comparable performance with VICON system [VIC]. [Supej, 2010] combines inertial sensors and GPS systems to measure skiing exercise.

Various algorithms are applied for activity classification. In [Mathie et al., 2004; Bao and Intille, 2004; Maurer et al., 2006], they use decision tree as the classifier. And in [Maurer et al., 2006; Bao and Intille, 2004], the author argues that decision tree outperforms or at least equivalent to Naive Bayes classifier. However in [Dougherty et al., 1995] the author argues that Naive Bayes outperforms in general classification problem. [Liu et al., 2009] uses dynamic time warping to recognize human gestures. [Ghasemzadeh et al., 2010] employs K-means to cluster different primitives and uses gaussian mixture model to build activity transcript.

[Mathie et al., 2004; Roetenberg et al., 2007; Ghasemzadeh et al., 2010] are performed in controlled laboratory environments. [Roetenberg et al., 2007; Roetenberg et al., 2009; Vlasic et al., 2007] have complicated system set up and carrying the system can potentially impede natural activities. Besides, certain sensors such as gyro, are not energy efficient and cannot provide effective continuous monitoring. Systems with those sensors need frequent configuration and provide a barrier for large community adoption. On the other hand, triaxial accelerometer is energy efficient and its ability in motion characterization has been validated in previous work.

The reliability and validity of accelerometer based wearable devices have been proved effective in characterizing post-stroke patients walking in [Saremi et al., 2006; Dobkin et al., 2011b]. Wearable sensor monitoring have shown to be complementary for performance evaluation and can be deployed for monitoring in the ambulatory community with feedback provided to the physicians and patients on a daily basis [Xu et al., 2011; Wang et al., 2011].

1.4 Organization

The rest chapters of this dissertation are organized as follows: In chapter 2, I describe a stepping based fitness evaluation system. In chapter 3, I describe individual behavior classification by sensor fusion, which covers the signal processing systems for a large scale clinical trial and the experience derived from deployment. In chapter 4, I introduce a visualization method of motion quality evolution, where I introduce a gait quality metric. In chapter 5, I extend the work of individualized classification into population based analysis. In particular, I propose a method of indexing accelerometer data, without critical information loss for motion analysis. Besides, I employ the hierarchical clustering algorithm to generate a library of primitive gait patterns for the stroke patients community. Chapter 5 summarizes this thesis, and discusses about directions

that I can further extend this thesis.

CHAPTER 2

StepFit: A Novel Fitness Evaluation System

2.1 Introduction

Physical activity and fitness promotion are central to the management and promotion of health and wellness. There exist numerous studies [Warburton et al., 2006; Fox, 1999] showing the effects of the physical activity and fitness on prevention of chronic diseases, premature death and improvement of mental well-being in the general population. Despite these broad benefits, many members of the population follow a sedentary lifestyle due to the constraints imposed by work and home life with little or no time dedicated to physical activity and fitness promotion. This is partially related to the costs associated with fitness assessment and advancement methods traditionally requiring expert trainer participation, fitness center access, expensive equipment and time.

The StepFit system exploits recent advances in wearable sensing and computation platforms to introduce low-cost systems for physiological monitoring, fitness assessment and feedback. StepFit systems can adapt to a user's schedule and can be deployed at the preferred location, not requiring additional exercise equipment.

Heart rate (HR) temporal response to variation in physical activity level is critical to fitness evaluation. Methods based on this principle have a rich set of applications ranging from assisted health to athletic fitness enhancement. For example, researchers of [Meersman, 1993] show higher HR variability (a metric of cardiac health) associated with higher fitness levels. While [Cole et al., 2000] shows the usage of the HR after a

maximal/submaximal exercise as a predictor of mortality.

This chapter describes StepFit - a low-cost, easy to set up, self-controlled and automated system for fitness evaluation, individualized physiological response modeling and prediction. StepFit enables automation of a category of standard fitness evaluation tests - step tests [Ryhming, 1954; McArdle et al., 1972; Hong et al., 2000; Shephard, 1966].

Step tests have been developed as a relatively simple alternative to measuring aerobic fitness requiring minimal available space or equipment. These now standard tests are performed by the subject stepping onto and off a platform of selected height h with a predetermined stepping frequency f over a period of a certain time t or until exhaustion. For example, in the Harvard Step Test (HST) [Brouha et al., 1943], exhaustion is defined as inability by the subject to maintain the selected stepping frequency for 15 consecutive seconds. Depending on the selected step test, the height of the bench, h, can be selected anywhere between 6-20 inches, while f and t also vary. This ensures that an appropriate step test can be selected in accordance with subject's fitness condition, biomechanical and age characteristics. StepFit automates any type of the step test, but in this chapter the HST [Brouha et al., 1943] is presented as an example. The following are the parameters of the HST: $h = 20$ *inches*, $t = 300$ *seconds*, $f = 0.5$ *steps/second*. Please note that for simplicity, in this paper we will refer interchangeably to the stepping frequency as the period during which the step occurs. These parameters, of course, are reciprocally related.

StepFit system consists of an HR sensor, motion sensor and a computational platform hosting algorithms for data aggregation, analysis and subject feedback. In addition to automation of the step tests, StepFit also models individual's HR response to each of the tests performed. The HR modeling in StepFit relies on using an exponential hyperbolic sine function that was shown to be effective in several formally conducted studies [Mizuo et al., 2000] where subjects performed constant workload activities. The

individual HR modeling can be used to analyze response of the subject across a variety of workloads (i.e. step frequencies) and predict individual's physiological response in the future.

The StepFit system advantages include:

1. Support for a variety of step tests adjusting to individuals with diverse biomechanical characteristics and age providing more accurate estimation of the aerobic fitness.

2. Automatic maintenance of the exact pace by generating a metronome like sound beat for every step, and monitoring the stepping technique by notifying the user in cases when actual stepping frequency is faster or lower.

3. Archival and processing of subject's physiological parameters, such as heart rate and motion.

4. Automated fitness score computation based on validated equation.

5. Modular design to support future automated recommendation development for individualized step aerobic exercise regimen based on subject's fitness performance, age and biomechanical characteristics. This capability is currently under development.

6. Unique capability for individualized HR modeling, prediction and assessment. This also enables determination of the maximal workload that should be recommended to the individual for fitness evaluation or exercise.

This chapter is structured as follows. Section 2.2 introduces the sensing platform, system diagram and user interface. Section 2.3 presents the algorithm for HR modeling and prediction, and addresses the signal processing module. Results are presented in Section 2.4. Conclusions and future work are addressed in Section 2.5.

2.2 System Overview

The StepFit system consists of the sensors (HR and motion), computation platform (including either netbook or a mobile phone) for sensor data processing and audiovisual user feedback, and a one height or adjustable height stepping platform.

2.2.1 Sensing Platform

Figure 2.1 shows the StepFit sensor system and experimental setup. Two types of sensors are used in StepFit - heart rate (HR) and motion. As shown on Figure 2.1a, HR monitoring system is based on the Polar chest strap [pol] and a Polar HR receiver module [oem] attached to a MicroLEAP [Au et al., 2007]. MicroLEAP is a Bluetooth enabled sensing platform with 8 ADC ports available for customized applications. Polar HR receiver module is connected to MicroLEAP through one of the ADC ports. Data from the chest strap is transmitted wirelessly to Polar HR receiver module using the Polar protocol, and then relayed by MicroLEAP via its Bluetooth interface to the computing platform (e.g. mobile phone or a laptop). The data from the HR chest strap is sampled with a frequency of 200Hz and then averaged by the computational platform at 1Hz, which provides the value of heart rate every second. This processing algorithm suppresses inherent measurement noise and outliers.

Motion is monitored by a tri-axial accelerometer, depicted at the lower left corner of Figure 2.1a. The tri-axial accelerometer sensor is connected to a second MicroLEAP platform through a set of ADC ports and data is relayed via Bluetooth to the computation platform. Note that the motion sensing unit (MicroLEAP platform with a tri-axial accelerometer) is developed on a flexible substrate, which makes it practical to be worn unobtrusively around the ankles or, as shown on Figure 2.1b, attached to subject's shoes. The MicroLEAP samples accelerometer with 100Hz, however, from our experimental results lower sampling frequencies, such as 40Hz, would also be adequate.

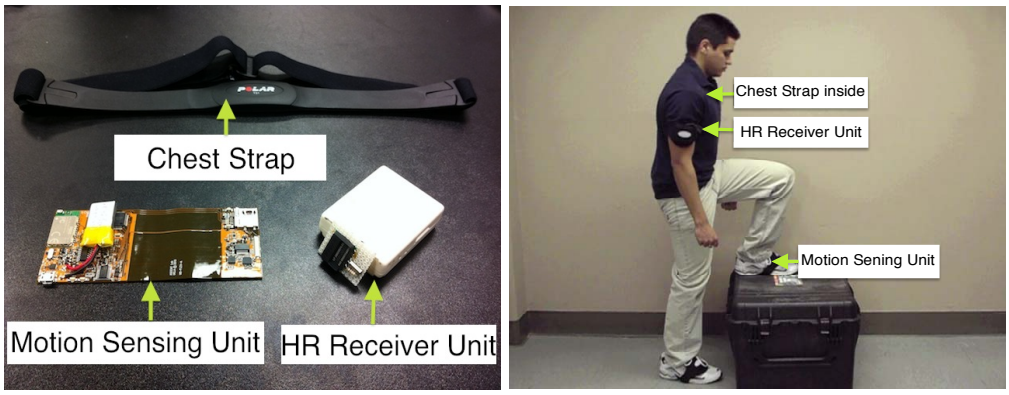

(a) (b)

Figure 2.1: StepFit sensor kit and experimental setup. (a) StepFit sensor kit including a flexible substrate, compact volume motion sensor at lower left. (b) Subject during fitness assessment by StepFit.

2.2.2 Harvard Step Test

As described in Section 2.1, StepFit is designed to automate each of the standard step tests. As noted, this paper emphasizes the Harvard Step Test (HST) [Brouha et al., 1943]. The HST is a simple-to-conduct and widely used test [Ryhming, 1954; Cullumbine et al., 1950; Lopez-S. et al., 1974; Stephenson et al., 1990] for aerobic fitness evaluation. The HST protocol calls for a subject to step on a 20-inch platform for 5 minutes or until exhaustion. Exhaustion is defined as not being able to maintain step frequency continuously for 15 seconds. In the presented system, one step is defined as alternating steps performed by the two feet in a complete cycle of "up-up-down-down". In the rest of the paper *step period* represents the time required to complete a step and *step frequency*, which is $1/$*step period*, represents the number of steps per second. Please note that when discussed in the context of exercise intensity, step period and step frequency can be used interchangeably as reciprocally related.

In order to guarantee that subject follows the prescribed step frequency (exercise intensity), a frequency monitor module is implemented. It automatically provides warn-

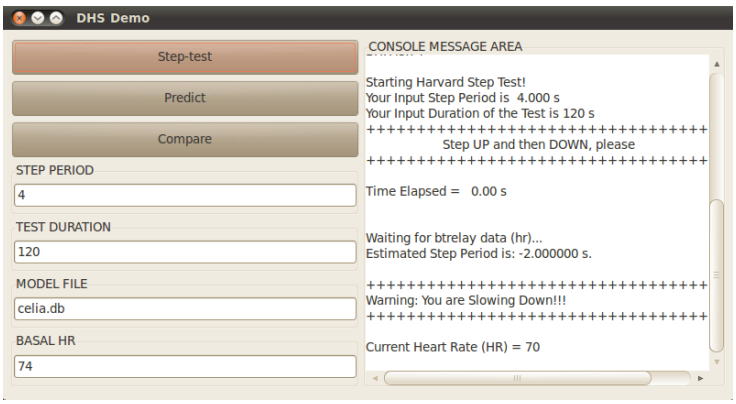

(a) GUI Interface

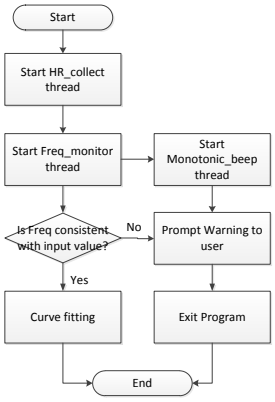

(b) HST routine flowchart

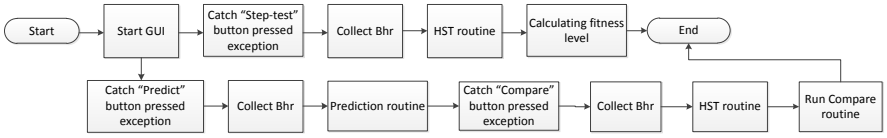

(c) System flowchart

Figure 2.2: StepFit system block diagram

ings if the subject deviates from the target frequency and terminates the test if the subject is unable to maintain stepping frequency for 15 seconds continuously (note that this threshold is the same as reaching exhaustion).

2.2.3 System Diagram and User Interface

Figure 2.2 shows the StepFit Graphical User Interface (GUI) and the information flow diagram in the system. The StepFit GUI and processing system is composed in Java to ensure portability to fixed and mobile platforms including Android platforms. When the StepFit application is executed, the GUI is displayed as shown on Figure 2.2a. This interface enables a selection of computing modules on upper left, user inputted test parameters on lower left and system real-time feedback on the right side panel. The computing modules include:

1. Step-test: Initiation of the HST routine.

2. Predict: Prediction of the individual's HR response based on the inputted parameters and individualized HR model database.

3. Compare: Comparison between the predicted and actual HR models(computed during the latest test).

The user inputted parameters include: STEP PERIOD - the target step period for the selected test (note that this is a measure of exercise intensity and reciprocally related to the step frequency); STEP DURATION - the predetermined duration of the selected step test; MODEL FILE - the personal database profile that will be used for prediction and also updated after every step test; BASAL HR - the basal heart rate derived by the system automatically before every step test.

As mentioned above, the panel on the right side of the GUI is dedicated to real-time feedback displaying current HR and motion information, guiding the user via audio cues when the next step needs to be taken and provides warnings in case the user performs the test incorrectly or is at the point of exertion.

StepFit information flow diagram is shown on Figure 2.2c. When StepFit application is initiated and the sensor systems are turned on, the computing platform automatically connects to the sensors via Bluetooth and generates appropriate sensor data profiles. At this point the StepFit GUI is displayed and the system is ready to operate. The user can then provide parameters, as described above, for the desired step test to be performed or for the prediction/compare functionality of the system.

If the subject presses "Step-test" button, the step test is initiated (e.g. Harvard Step Test in the example of this paper). As shown on Figure 2.2c, basal or resting heart rate (Bhr) is first recorded. Bhr is defined as an average value of individual's heart rate that does not vary significantly in time. Once the Bhr is determined, system initiates a step test routine (HST routine). Figure 2.2b shows a block diagram of the HST routine. The

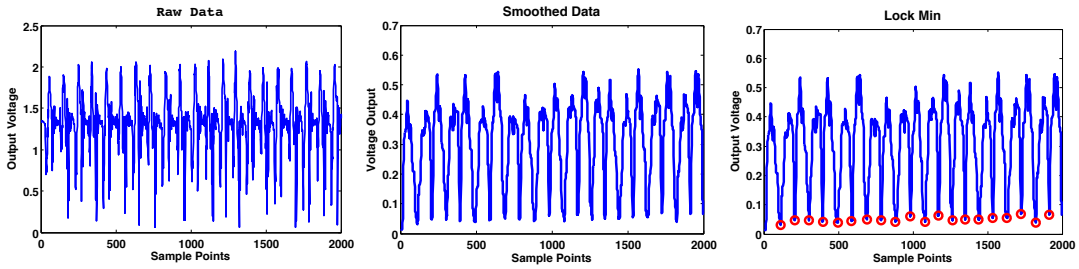

Figure 2.3: Signal processing of motion data in StepFit

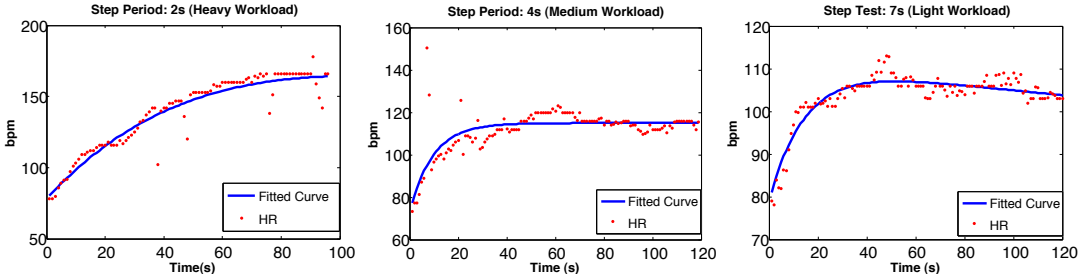

Figure 2.4: Curve fitting with different workloads in StepFit

HST routine records HR and monitors step frequency simultaneously. In parallel, the computing platform initiates a metronome like audio signals and text outputs to assist subject with correctly following the selected step frequency. Each sound or system notification corresponds to 1/4 of a complete step cycle, i.e. steps performed by either of the legs up or down.

If the step frequency deviates from the target value, a warning message is generated on the screen and played via audio to assist the subject to speed up or slow down their step rate. If the subject cannot adjust the step rate accordingly and the warnings persist for 15 consecutive seconds, the test is terminated and the system assumes subject reached exertion. Otherwise, the HST routine completes the test when the parameter inputted in TEST DURATION is reached.

At the end of the HST routine the StepFit system models the individual HR response to the exercise intensity of the test and computes the fitness score using the standard HST model. The HR model (some examples are shown on Figure 2.4) and the fitness

score (refer to Figure 2.5) are displayed for individualized feedback. Furthermore, user's database file is updated with the latest HR model.

If the subject presses "Predict" button, then prediction routine is initiated. This routine enables prediction of the HR response with changes in workloads (i.e. step period or frequency), which is a valuable analytical tool in studying performance. During prediction phase, the system applies interpolation/extrapolation using parameters of models archived in user's database file. Due to space limitation, further discussion of the prediction capability and corresponding results are not included in this paper.

If the subject presses "Compare" button, validation of the prediction capability of the system with the actual performance during the step test is performed. As can be noted from Figure 2.2c, the system predicts the HR response using provided parameters and then initiates a step test to collect the latest fitness data from the subject. Once the step test completes, the statistics are displayed showing accuracy of the prediction method. Note, however, that the accuracy of system prediction improves as the user's database increases the number of collected models.

2.3 Algorithm Design

2.3.1 Heart Rate Modeling

Given a constant workload, such as step frequency, the HR response was shown to be accurately modeled with an exponential hyperbolic sine function [Mizuo et al., 2000]. This function can be defined by Eqn.2.1, where *HR* represents heart rate (in bpm) at time *t* and *Bhr* represents basal heart rate (in bpm) before the exercise. The coefficients in the equation (i.e. α, β and ω) do not have physiological meaning and vary with different workloads and individual characteristics.

$$\text{HR} = \text{Bhr} + \alpha \cdot e^{-\beta \cdot t} \sinh(\omega \cdot t) \tag{2.1}$$

The nonlinear HR curve fitting is realized by using the Levenberg-Marquardt minimization routine [Press and Flannery, 1988].

2.3.2 Frequency Monitoring

As described above, the StepFit system provides automated warnings when the user deviates from the selected constant workload (e.g. step frequency or period). This is accomplished by processing motion sensor data and computing the exact step frequency during the step test. In the presented system the frequency analysis is performed on the dominant axis of the motion sensors.

The real-time data is stored in a temporary buffer and has a minimal length of *L*, defined as $L = 2 * \textit{step period} * \textit{sample rate}$. The buffered data spans a time window from the current motion sample to *L* previous samples. This guarantees that at least two step cycles can be captured in the buffer. The minimal length setting is applied to ensure that historical data will not dominate changes in current data.

Next, the offset is removed from the raw data, followed by a moving-average smoothing filter. Smoothing removes coupled high frequency noise in the data. Finally, a piece-wise local minimum function is employed to find local minima point [loc]. The search piece however has to be carefully selected. It is closely correlated with the stepping frequency.

Figure 2.3a shows the raw stepping data with frequency of 0.5 steps/second (step period of 2), Figure 2.3b shows this data after smoothing and Figure 2.3c shows the selected local minima values.

Finally, adherence to the step frequency is determined as practical variations within 20% from the target. Deviations above or below then result in appropriate warning

messages generated by the StepFit system.

Note that this approach was experimentally validated to be robust in practice. Furthermore, due to its simplicity, these algorithms can be implemented in the microprocessor of the MicroLEAP sensor nodes, if the computation platform has limited capabilities or to reduce communication overhead between sensors and the platform.

2.3.3 Prediction Method

The prediction routine algorithm performs a search through the user's HR model database for a match using the step frequency parameter (exercise intensity). If such a match is discovered, the database entry is used for prediction. Otherwise, interpolation and extrapolation are employed relying on the user's database models in the immediate vicinity of the desired step frequency parameters.

2.4 Results

As described above, StepFit is a system that automates existing and well validated fitness assessment (e.g. step tests) and HR modeling technique (for example, exponential hyperbolic sine function). Therefore, this section presents several proof of concept validation results that demonstrate functionality of the system.

2.4.1 HR vs Workload

Depending on individual user characteristics and selected workloads, the heart rate response and the corresponding model will exhibit substantially different trajectories. As shown on Figure 2.4, HR response to constant workload can be divided broadly into 3 categories associated with exercise intensity: heavy, medium and light. For each of these exercise intensity categories, HR response has unique properties. As can be noted

from Figure 2.4a, for a heavy workload, the HR response has a tendency to increase after an initial sharping rising phase. For a medium workload, the HR response tends to stabilize after the initial rising phase (refer to Figure 2.4b). Finally, for the light workload, the curve tends to eventually decrease, as shown on Figure 2.4c. Important to note that for individuals with diverse biomechanical characteristics, fitness level or age, the stepping frequency correspondence to the 3 different classes of workloads may be different. Therefore, focusing on individualized HR modeling and fitness optimization is critical and can be determined by the StepFit system analysis.

Table 2.1 shows the HR modeling performed by StepFit for five subjects with 3 different workloads (step frequencies or step periods). Note that the diversity in the model parameters, which accentuates the need for individualization.

Another proof of concept evaluation of StepFit was performed with an individual subjected to a variety of different workloads. Table 2.2 shows the HR profiles for this individual under different step frequencies (step periods). The residual, which shows the accuracy of HR modeling, is relatively small, especially noting that HR deviations within 10bpm are considered normal when comparing different sensors. This accentuates the practical application of the exponential hyperbolic sine function to modeling HR response during the step test. The residual is defined in Eqn.2.2, where *N* represents the total number of points used for modeling, C_{fit} represents the fitted curve and C_{real} represents the actual HR response during the test.

$$\text{Residual} = \frac{1}{N}\sum_{i=1}^{N}[C_{fit}(i) - C_{real}(i)]^2 \tag{2.2}$$

2.4.2 Fitness Index

Once the subject completes the selected step test, the StepFit system computes the fitness index score based on the standardized and validated measures of aerobic exercise capacity and heart rate recovery. The score formulation is defined in Eqn.2.3 [Johnson

Table 2.1: Multiple Subjects' Profile Comparison

Subject	Workload	Bhr	α	β	ω	Residual
No.1	2s	78	940.3	0.009700	0.002400	10.37
	4s	73	83.91	0.05180	0.05180	11.98
	7s	79	65.37	0.03500	0.03270	6.507
No.2	2s	84	95.77	0.05810	0.06100	7.605
	4s	92	55.63	0.09680	0.09610	9.795
	7s	87	51.01	0.08550	0.08690	6.852
No.3	2s	65	75.43	0.1043	0.1077	12.91
	4s	61	46.96	0.05100	0.05010	9.391
	7s	58	48.05	0.03880	0.04030	9.702
No.4	2s	103	112.02	0.01440	0.01720	5.590
	4s	88	91.53	0.04910	0.04940	7.396
	7s	104	37.10	0.03530	0.04010	7.865
No.5	2s	75	130.5	0.01480	0.01520	4.204
	4s	63	82.14	0.02450	0.02340	5.690
	7s	84	29.18	0.06200	0.06250	6.4495

Table 2.2: A Subject's Heart Rate Profile vs. Workloads

Step Period	Bhr	α	β	ω	Duration	Residual
2s	78	940.3	0.0097	0.0024	96	10.37
3s	67	144.7	0.0314	0.0343	120	13.92
4s	73	83.90	0.0518	0.0518	119	11.98
5s	71	86.97	0.044	0.0413	120	7.540
6s	78	68.77	0.0394	0.0390	120	5.681
7s	79	65.37	0.035	0.0327	120	6.507

Figure 2.5: Fitness index generated by StepFit

Table 2.3: Fitness Index Table

Rating	Fitness Index
Excellent	>90
Good	80 to 89
High average	65 to 79
Low average	55 to 64
Poor	<55

et al., 1942], where the *Exercise Duration* is either the selected duration of the test or time to exhaustion, *Recovery Beats* are computed as the sum of heart beats 1 to 1.5 minutes after the test, plus the beats 2 to 2.5 minutes after the test, plus the beats 3 to 3.5 minutes after the test. For Harvard Step Test, the fitness index is only evaluated with step period of 2 seconds (i.e. step frequency of 0.5).

Table.2.3 shows the standard fitness index values and the corresponding aerobic ratings. Figure 2.5 shows the fitness index feedback generated by the StepFit system for one of the subjects.

$$\text{Fitness Index} = \frac{100 \times \text{Exercise Duration}}{2 \times \text{Recovery Beats}} \tag{2.3}$$

2.5 Conclusion and Future Work

Fitness evaluation and promotion are critical measures for preventing disease and promoting health and wellness on a large population scale at low cost. This chapter presented StepFit - an automated self-administered, low cost and convenient system for fitness evaluation, heart rate response analysis and prediction. The StepFit system consists of unobtrusive low cost HR and motion sensors, and a computational platform that is used for data processing, archival and user feedback. The system automates step tests (for example, the widely applied Harvard Step Test), which are standardized fitness evaluation techniques that are extensively validated in diverse subject populations. By introducing automation and networked data acquisition, StepFit directly resolves a challenge in deployment of the step test that otherwise requires the presence of trained personnel.

The StepFit system assists a user in performing the step test by automatically performing the physiological data collection, ensuring the test duration and monitoring the stepping technique by evaluating subject's step frequency. The system also performs accurate HR modeling based on the validated exponential hyperbolic sine function model. The HR models are archived in the individualized databases which can be used for HR analysis and prediction of physiological response to changing workload demands.

In our current and future work, we have partnered with the UCLA Exercise Physiology Laboratory from the School of Medicine to augment the StepFit system with an automated fitness prescription method. This method will individually determine exercise intensity (step frequency), bench height and exercise duration based on the results of the test, biomechanical characteristics of the individual, age, gender, preexisting medical conditions and the desired fitness target.

CHAPTER 3

Precise Classification of Individual Behavior by Sensor Fusion

3.1 Introduction

Nationwide, more than 4 million stroke survivors are suffering from after-effects. The average cost of care for a patient up to 90 days after the stroke incident is $15,000 and 16% is spent on rehabilitation and 14% is on physician [Association].

Continuous monitoring of human motion and behavior are central to healthcare for advancing neurological rehabilitation, ensuring adherence to fitness promotion protocols, enabling activity-based interventions for hypertension and many others. Most importantly, the introduction of robust monitoring of complex subject motion can enable the first direct measurement and assurance of outcomes for treatment for patients that have left the clinic and are now in residential or workplace environments where the rehabilitation and treatment must continue effectively.

Due to recent advancements in low-power, energy efficient, non-intrusive, compact motion sensing devices, the deployment of large scale wearable systems is now practical at low cost. As this thesis will describe, this can be combined with convenient energy recharges, data acquisition and transport that has proven effective now at the national and international scale. A critical need exists for technology that harnesses time and frequency domain signal processing technology and machine learning principles to provide classification capability for complex motion. This is particularly important for

characterization of subjects that are afflicted with neurological disorders (for example stroke that introduces hemiparetic gait) or complex motion impairments resulting from Parkinson's disease and multiple sclerosis. Finally, it is essential to note that it is now required to provide accurate classification of motion for individuals in the community and outside of laboratory facilities.

3.2 WHSFT: Wireless Health Sensor Fusion Toolkit

3.2.1 The Software

Wireless health sensor fusion toolkit (WHSFT) is a modularized matlab software that aims at general pattern recognition of time series data. It has a supervised learning framework. It has extendible code structure for adding new features and classifiers. Currently WHSFT support Nave Bayes and Decision Tree classifier.

The graphic interface is shown in figure 3.1.

WHSFT includes four parts: merging, labeling, training and testing. The merging tool is in charge of concatenating data from multiple files and combining multiple sensors data, as well as aligning time over multiple sensors. The labeling tool is in charge of labeling different states in training. The training tool allows selection of preferred classifier, selection of feature combinations and generating feature distribution of training. The testing tool generates classification result on testing data as well as confusion matrix, based on training structure.

3.2.2 Classification Results from WHSFT

WHSFT is validated by both controlled laboratory experiment and community activity classification. In the experiments, I use leave-one-out cross-validation method to check the performance of WHSFT. The subjects wear triaxial accelerometer sensors on both

Figure 3.1: WHSFT graphical user interface

wrists and ankles.

3.2.2.1 Controlled Laboratory Validation

In controlled laboratory experiment, we collect data from normal subjects, including both upper extremity activities and lower extremity activities. The activities include walking, running, upstairs, downstairs, eating, reaching out, combing hair, cycling, rest, etc. Those activities are performed purposefully and repetitively.

The classifier for this validationa is Naive Bayes classifier. And the sensing platform is accelerometer based. Figure 3.2a shows the raw data and classification result of locomotion, and figure 3.2b shows the raw data and classification result of upper extremity activities. As mentioned earlier, WHSPFT is a general pattern recognition software. So there is no limitations or requirements for the choice of activities/states. It can be observed from the classification result that WHSFT can classify activities with

a high accuracy, even activities done at different trials.

3.2.2.2 Ambulatory Daily Activities Classification

With the first step validated results got from controlled laboratory condition, we further apply it to patients suffering from multiple sclerosis (MS). The sensing platform is accelerometer based. And they are worn on both wrists and both ankles. We compare the classification result with a standard user-annotated log. The user checks the activities within the log and writes down the start and end time. Since we aim at characterizing the patients' daily life, we have a bigger training set and it includes the following activities.

- Dressing: Put on and take off a uniform outwear
- Feeding: Imitate feeding using a uniform spoon
- Picking: Stand and turn a circle, then pick up a penny on the floor
- Fetching: Take a book on a high shelf and put back
- Reaching: Reach a uniform cup placed remotely on a table
- Walking: Walk through the hall way
- Stand up and sit down: Walk a short distance and sit on the chair, then stand up and walk out, then walk back and sit down
- Stair Ascent: climb up one floor of stair, guarded by doctors
- Stair Descent: climb down one floor of stair, guarded by doctors

The activities included in the printed activity log are

- Brushing teeth

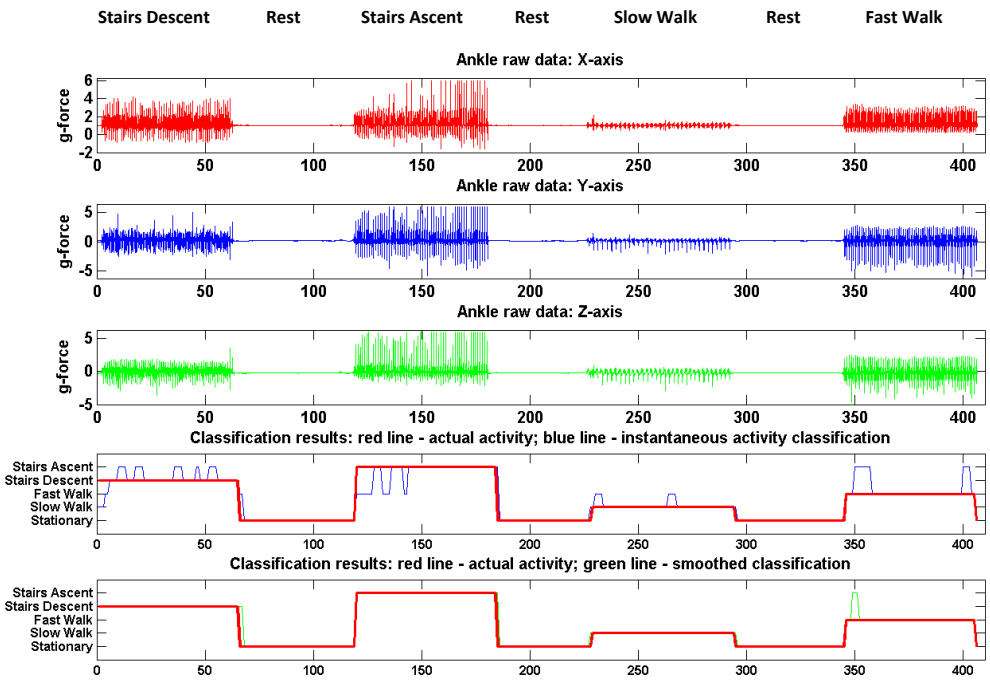

(a) Lower extremities activity

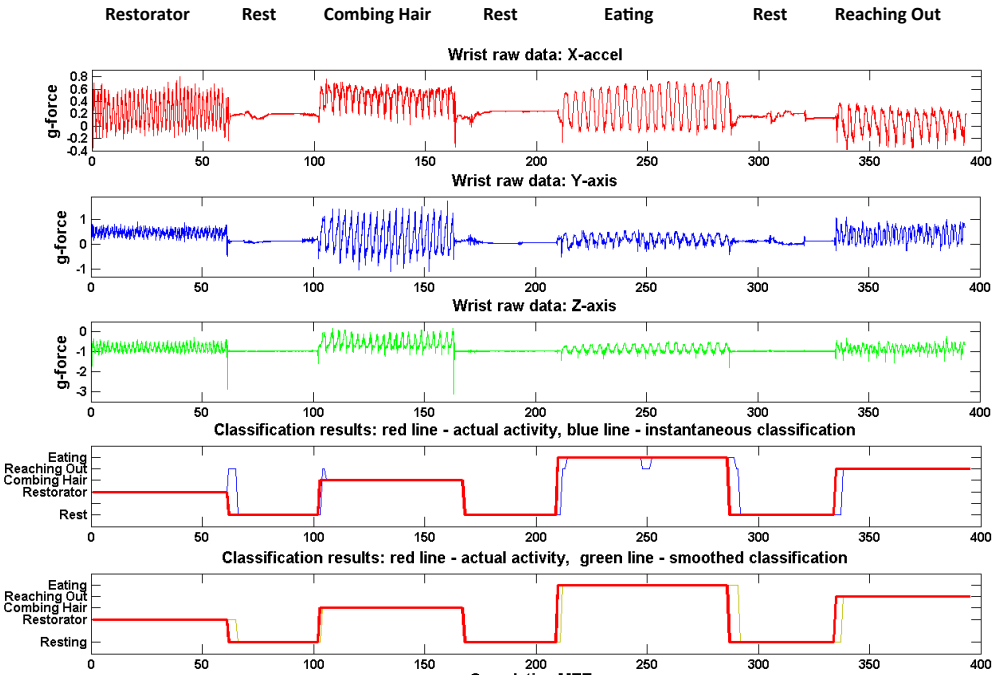

(b) Upper extremities activity

Figure 3.2: Classification results

- Dressing/undressing
- Walking
- Climbing stairs
- Preparing mean
- Eating
- Washing dishes
- Sitting/watching TV/reading
- Computer/paperwork
- Light cleaning
- Vacuuming/heavy cleaning
- Driving
- Shopping
- Sleeping/napping
- Exercise (stretching(A), strengthening(B), cardio(C))

Figure 3.3 shows the classification result, the user annotated log file and raw data for upper extremity activities and figure 3.4 shows the classification result and user-annotated result for lower body activities.

When we plot the user-annotated information, for upper extremity activities, we combine ”brushing teeth” and ”eating” into ”feeding-type”. And combining ”sitting/watching TV/reading” and ”computer/paperwork” into writing type. The reason we do this is because due to brief duration of those activities and unrepetitive properties, it’s hard to

get reliable frame-based features. So the classification result is derived largely by the amplitude of the activity, rather than specific state. The figures indicate that the classification can indicate some information out of ambulatory daily life.

It can also be observed that the subject can skip a significant amount of information in checking the log, and he can extend the duration of annotated activities for not being conscious of that. It's actually too much work for a subject to maintain the log information and behaves as normal life. In order to solve this problem, we narrow down the set of interested activities for lower body activities and describe activities of upper extremity by their functionality.

3.3 Hybrid Gait Classification System

3.3.1 The Algorithm

Classification of gait for patients is a challenging task, due to the diversity of temporal and spatial properties of gait traces. Figure 3.5 a shows an episode of gait from a healthy subject with normal gait; b shows an episode of gait from a stroke patient with hemiparetic gait. The signals from the normal subject are repetitive, consistent and strong. However, signals from the patient are weak on the hemiparetic side and have episodic irregular cycles, even on the less affected limb (it is right ankle in this example). Diversity of gait not only exist among individuals, but also within an episode of walking from the same subject. Besides,

The In order to solve challenges of diversity and volatile signals from patients, this thesis introduces an individualized hybrid classification method. The gait classification is accomplished with a novel hybrid approach based on a multi-tier combination of Naive Bayes [Bishop, 2006] and Dynamic Time Warping [Sakoe and Chiba, 1990] for subject state classification. In this thesis the results of the hybrid system classification are presented and show a significant improvement in accuracy over either a purely

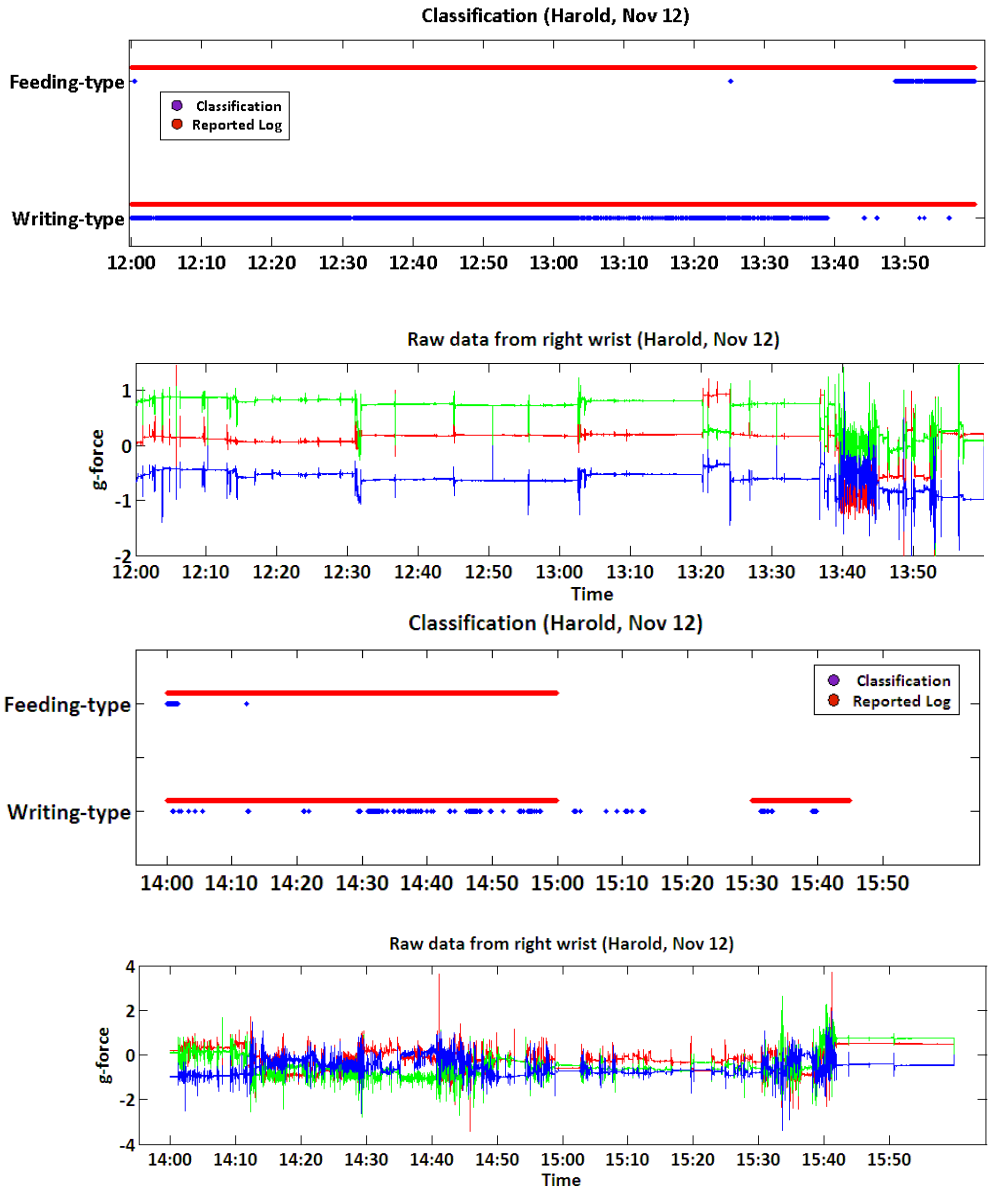

Figure 3.3: Upper body activities classification. It includes raw accelerometer data, annotated log record by patient and classification result

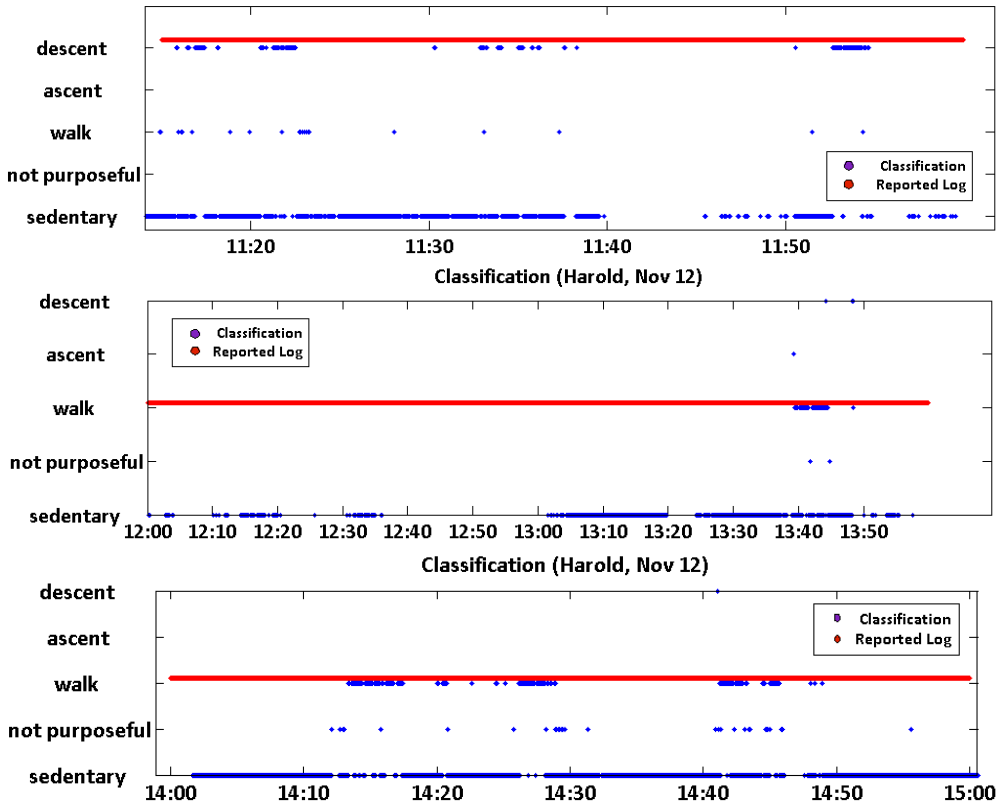

Figure 3.4: Lower body activities classification. It includes raw accelerometer data, annotated log record by patient and classification result

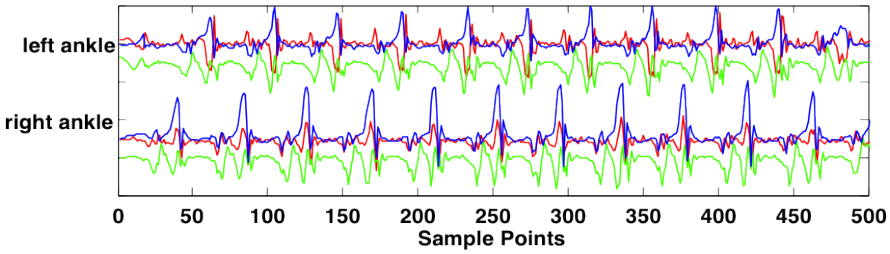

(a) Normal Gait

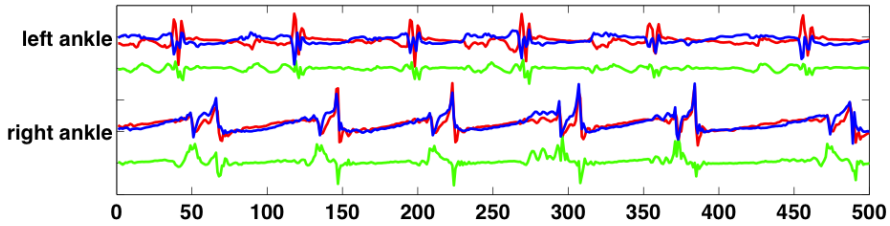

(b) Hemiparetic Gait

Figure 3.5: Gait comparison between healthy subject and stroke subject

Naive Bayes or Dynamic Time Warping approach. These results are achieved by combining the capabilities and output from both algorithms in such a way as to maximize the confidence of classification and increasing classification accuracy.

The system belongs to a supervised learning category - it creates a model from the test data based on collecting individualized templates and probabilistic activity state parameters. The system can then apply this model to classify activity in a testing data set. Note that classification approach of the described system is individualized to every subject. Therefore, the system is effectively tuned to every individual.

In [Bao and Intille, 2004] authors argue that the best classifier for human activity is a decision tree. Note, however, that in the system described in this thesis the detection of the gait activity is identical to a one-step decision tree, therefore, the approach is as effective.

Naive Bayes [Bishop, 2006] is a powerful probabilistic classifier operating under assmuption of feature independence. Features can be thought of as statistically unique

elements of the sensor data, which are used to differentiate diverse classes or states. In the presented system, classes/states are the different user activities of interest, such as walking. In reality the independence assumption is either natural to a given problem or independence can be achieved by data manipulation. The Naive Bayes formulation is presented in Eqn.3.1, where **C** represents classes/states and **F** is a feature vector. When the feature set is determined, $p(F_1...F_n)$is a constant, $p(C)$ is a prior, typically uniformly distributed, probability. The posterior probability $p(C|F_1...F_n)$ is determined by the likelihood $\prod_{i=1}^{n} p(F_i|C)$ (the trained model), as shown in Eqn.3.2.

$$p(C|F_1...F_n) = \frac{p(C)\prod_{i=1}^{n} p(F_i|C)}{p(F_1...F_n)} \tag{3.1}$$

$$\arg\max_C p(C|F_1...F_n) = \arg\max_C \prod_{i=1}^{n} p(F_i|C) \tag{3.2}$$

$$= \arg\max_C \prod_i \frac{1}{\sigma_i} e^{-\frac{1}{2}\frac{(F_i-\mu_i)^2}{(\sigma_i)^2}} \tag{3.3}$$

In the system described in this paper, the distribution of class C is fit to a multivariate gaussian distribution with each feature serving as a random variable. Eqn.3.2 could be rewritten as Eqn.3.3. We can further modify Eqn.3.3 by taking the log from both sides to obtain Eqn.3.4. This can be further simplified to yield Eqn.3.5 and Eqn.3.6.

In Eqn.3.5 Λ represents diagonal covariance matrix for features and f is a feature variable. Let $\Lambda^{-\frac{1}{2}}(f-\mu) = y$, then Eqn.3.5 can be written as Eqn.3.6. Since $\Lambda^{-\frac{1}{2}}(f-\mu)$ is a normal gaussian distribution, y^2 is χ^2 distribution with $|\mathbf{F}|$ degrees of freedom (where $|\mathbf{F}|$ is the number of features).

$$\log p(C|F_1...F_n) = \log \prod \frac{1}{\sigma_i} e^{-\frac{1}{2}\frac{(F_i-\mu_i)^2}{(\sigma_i)^2}} \tag{3.4}$$

$$= -\Sigma \log \sigma_i - \frac{1}{2}\Sigma \frac{(F_i-\mu_i)^2}{\sigma_i^2}$$

$$= -\frac{1}{2}\log \det \Lambda - \frac{1}{2}(f-\mu)^T \Lambda^{-1}(f-\mu) \tag{3.5}$$

$$= -\frac{1}{2}\log \det \Lambda - \frac{1}{2}(y)^2 \tag{3.6}$$

It is now possible to determine a threshold by assuming that only 5% of the left most distribution can be misclassified, which is determined empirically. The process is derived in Eqn.3.7, Eqn.3.8, Eqn.3.9 and Eqn.3.10. In Eqn.3.10, F_F^{-1} represents the reverse χ^2 distribution and the lower $|\mathbf{F}|$ represents the number of freedoms.

$$P(-\frac{1}{2}\log det\Lambda - \frac{1}{2}y^2 > T) = 0.95 \tag{3.7}$$

$$P(y^2 < -2T_i - \log det\Lambda) = 0.95 \tag{3.8}$$

$$-2T - \log det\Lambda = F_F^{-1}(0.95) \tag{3.9}$$

$$T = -\frac{1}{2}F_F^{-1}(0.95) - \frac{1}{2}\log det\Lambda \tag{3.10}$$

The feature set for Naive Bayes classifier with application to detection of the ”walking” state includes: standard deviation of three axis, correlation between every two axes and mean value of y axis (y axis is pointing downward to ground). This set was determined to be effective from empirical validation.

Dynamic time warping (DTW) is an algorithm to measure similarity between time series. The algorithm will return a metric that summarizes the euclidean distance along the warping path. Introduction of DTW is to leverage the effects of amplitude variance and speed variance of the time series signal. Figure 3.6 shows two accelerometer traces that correspond to a stride cycle of fast walk and slow walk.

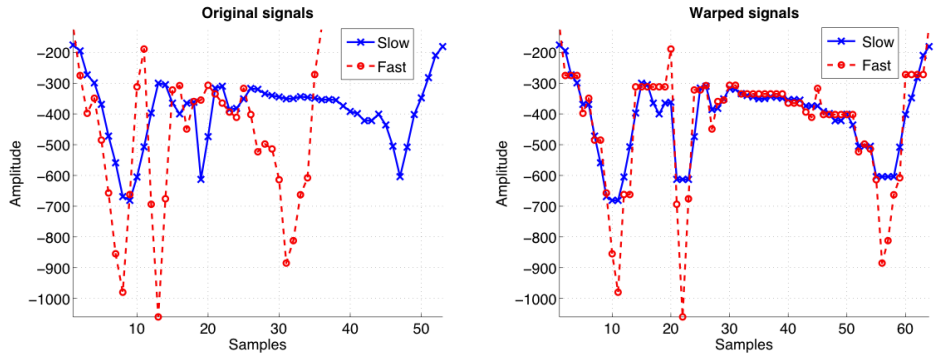

Figure 3.6: DTW result on walking cycles with different speed. The left figure is the original signal and right figure is DTW aligned signal

The data is first analyzed by the DTW classifier for a coarse characterization. DTW classifier takes a pre-saved, complete walking cycle from training data as a template. The matching score is set relatively low in order to identify all of the potential walking segments. Since the shape matching is cycle based, the processing window is set to a value comparable to the length of the template, with 50% stepping overlap.

Next, the data is analyzed by the Naive Bayes (NB) classifier for a fine-grained characterization. The NB classifier is described above and in the proposed implementation the processing window for the testing data was experimentally selected to be 4 seconds in order to include at least one cycle of activity. The processing window also steps with 75% overlap to ensure data stability.

Results from DTW and NB classifiers are combined using Algorithm (1). Labels from NB classifier are always assumed to be correct due to a high confidence of detection. If a consecutive label section returned from DTW is shorter than the processing window of NB the labels are considered correct. If a consecutive label section from DTW also matches with at least one high confidence label produced by NB, then the complete label segment is counted as correctly classified. In all other situations the classified output is ignored since a match between the outputs of the two algorithms has not occurred.

Algorithm 1 Combine Label from DTW and NB

Input: Label sections: {NBsection, DTWsection},

Output: Label positions $L = zeros(1, len)$

$L = NBsection$

for $t \leftarrow 1$ to len **do**

  if $DTWsection(i) \leq NBwindow \cup length(NBsection(i) == 1) \geq 1$ **then**

    $L = DTWsection(i)$

3.3.2 Performance Evaluation

In collaboration with Dr. Bruce Dobkin (Neurology Department at the UCLA School of Medicine), six subjects recovering from stroke were selected. Each subject developed a hemiparetic gait in walking as a result of stroke. An appropriate UCLA IRB and the subject consent approvals were obtained before the experiments. Subjects were in a diverse age range from 42 to 74, with a standard deviation of 10.9. Four of the subjects were males and two were females. Note that the described system is individualized, therefore, a pool of 6 subjects is adequate for early system performance evaluation.

For training data collection each subject was asked to walk through a marked and observed 50-foot section with three different safe speeds selected by subjects. Next, the subjects were escorted by Dr. Dobkin to walk a predetermined distance with preferred speed, but without observation by the engineering team. Dr. Dobkin, however, was manually collecting the groundtruth data. This was called a blind test and reported in this paper for speed computation validation. Finally, subjects were asked to wear devices for a complete day, while they were released from the hospital.

The subjects returned the MDAWN devices after a day of usage in the community or home. The data was uploaded and automatically analized by the classification system. In order to obtain an accurate groundtruth measure for comparison of the results an expert trained in recognizing human motion data from the raw accelerometer pro-

Table 3.1: Performance Comparison Summary

classifiers	accuracy%	precision%	recall%
Hierarchical	97.31±0.530	83.61±5.310	84.38±6.620
DTW	93.37±1.695	60.43±10.63	89.30±4.190
NB	93.73±1.760	87.28±9.907	37.75±20.60

files was asked to manually count all of the walking periods for every subject. Table 3.1 shows the classification accuracy comparison between the hierarchical system described in this paper, pure DTW and NB. As can be noted from the table, the proposed hierarchical approach outperforms both DTW and NB with higher accuracy and lower standard deviation in classification.

Consider the results presented in the table - notice that the NB classifier achieves high precision while DTW achieves high recall. This accentuates the benefit in combining the two approaches, while mitigating shortcomings - NB classifier has a low rate in false positives but high rate in false negatives, while DTW exhibits an opposite behavior.

3.4 Kinematic Characterization of Gait

After identifying the activity sections, the next step is kinematic characterization of gait. Kinematic parameters such as speed, cadence, stride length and swing ratio are critical outcome measures and calculated at this stage. Figure 3.7 shows the graphic interpretation of gait cycles. It depicts a complete stride cycle, starting with heal striking (when the foot contacts the ground) and ending with the next heal striking. Each cycle begins at initial contact with a stance phase and proceeds through a swing phase until the cycle ends with the limb's next initial contact. The swing and stance phases are separated by toe-off.

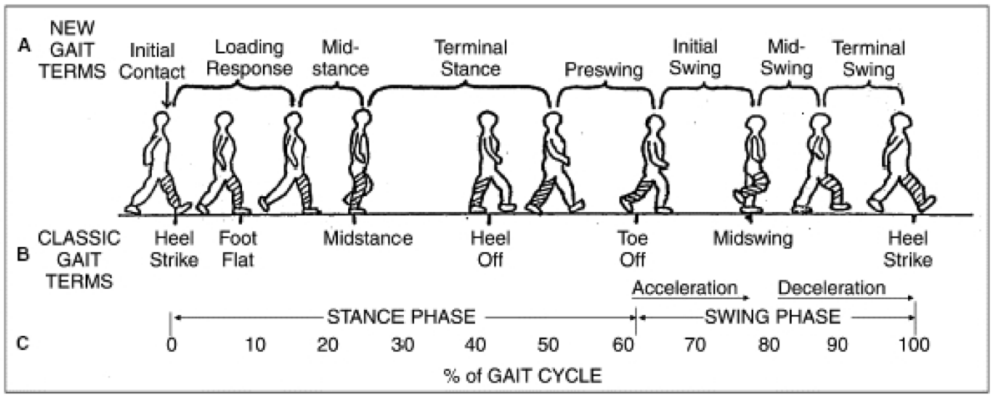

Figure 3.7: Gait graphic interpretation [Cuccurullo, 2004]

The critical phases (such as swing and stance) and critical events (such as heal striking and toe-off) can be found in accelerometer traces as well. Figure 3.8 shows the stride segmentation of accelerometer signals. Sensor are worn on the inner side of shank, two fingers above the ankle bone; x and z axes are on the horizontal plane, while y axis is pointing downwards to ground. The accelerometer readings of the stance phase accord with basic physics since no distinct fluctuations observed. When the first distinct acceleration shows up, it corresponds to the event of toe off and enters the swing phase.

3.4.1 Peak Detection

In order to finely characterize motion kinematics, it is critical to first isolate each stride unit. Peak detection is employed to stamp individual strides and thus provides boundary information. A metric, defined as $P_{val} = \sqrt{x^2 + y^2}$, is introduced. It is signal composition of x and z axes to represent data confidence. This variable magnifies a unique sub phase defined as in swing, where absolute values of x and z achieve maximum, as shown in figure 3.8 at time 0.5s of left ankle signal, while suppresses other phases within a stride. Peak positions are determined by a local maxima algorithm [loc] with P_{val} and $windowsize$ as inputs. $windowsize$ is determined by adaptive thresholds, according to the strength of P_{val}. Higher peak values usually represent higher

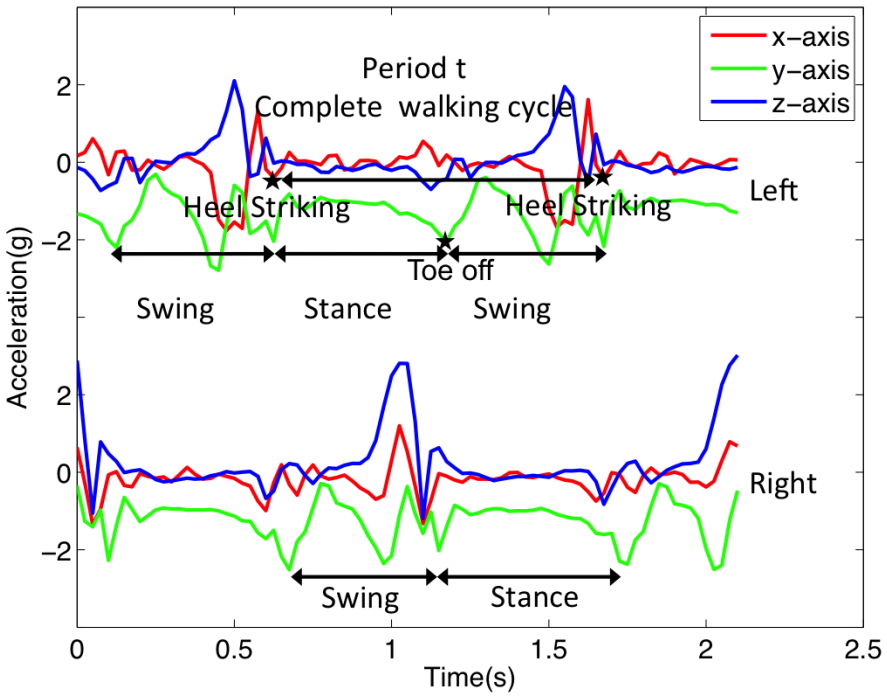

Figure 3.8: Stride segmentation of accelerometer signal

speeds, in which case smaller window size is needed, and vice versa. Figure 3.9 shows an example of peak detection from a normal subject.

Gait by nature is alternative. So consecutive heal striking of left leg provides the boundaries for the right leg and vice versa. As can be validated by [Cuccurullo, 2004], the walking cycle of left leg will affirmatively include a complete swing phase of the right leg (however, not necessarily include the right leg stance period), for example in figure 3.8. The algorithm switches the peaks between left leg and right leg as stride boundary information.

For patients with hemiparesis, the metric P_{val} may not achieve maximum at the pre-defined position from the impaired limb data and thus cannot provide reliable position for the boundary of the less-affected stride. Typically multiple local maxima are found (caused by both swing and heal striking) by applying the peak detection purely. According to the stride boundary of impaired limb derived by peak detection from the

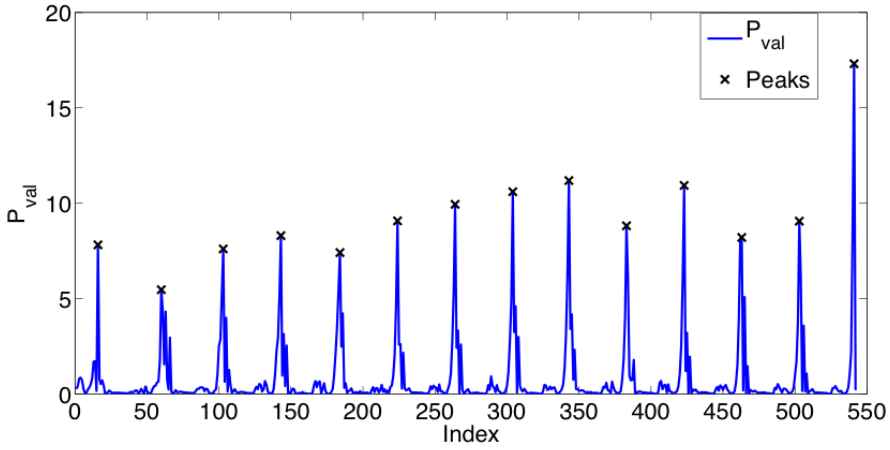

Figure 3.9: Peak detection for gait

less-affected limb, a local maxima array that belongs to the same stride is known. Since heal striking happens after swing, the local maximum that is the end of local maxima array is natural to be heal striking from the impaired limb. In this way, boundary for the less-affected leg are derived. An alternative method, however, is to shift the peaks half of the walking cycle period to get boundaries for the less-affected leg. This is based on the alternating feature of gait.

Accuracy of peak detection is the basis for kinematic modeling. I inspect 524 strides from 26 patients, including patients with diverse gait, from very capable to very disabled. Of all, 6 peaks are mislabeled (5 false negatives and 1 false positive) and the accuracy is 98.85%.

3.4.2 Orientation Correction

In SIRRACT setting, the sensor is mounted in the inner side of shank, two fingers above the ankle bone [Xu et al., 2011]. When it is mounted properly and the subject is vertically sedentary, the readings from x, y, z axes should be close to $[0; -1; 0]$(x and z axes are on the horizontal plane, while y axis is pointing downwards), as figure 3.10 a showed; we call this state sedentary state. In the case of inappropriate mounting,

in sedentary state, the values are deviated and an example is shown in figure 3.10 b. The sensor in this case can be modeled as rotated Euler angles $[\phi; \theta; \psi]$(Here we don't consider translation).

We name the SIRRACT setting coordinate frame $o_0x_0y_0z_0$ and use it as a reference frame; name the rotated coordinate frame $o_1x_1y_1z_1$. Let P represent an array of points in space and it has coordinates P^0 in frame $o_0x_0y_0z_0$ and P^1 in $o_1x_1y_1z_1$. According to homogeneous transformation, $P^0 = R_1^0 * P^1$. R is the rotation matrix that can be factorized into $R_z(\psi)R_y(\theta)R_x(\phi)$, which equals to:

$$\begin{pmatrix} \cos\theta\cos\psi & -\cos\phi\sin\psi + \sin\phi\sin\theta\cos\psi & \sin\phi\sin\psi + \cos\phi\sin\theta\cos\psi \\ \cos\theta\sin\psi & \cos\phi\cos\psi + \sin\phi\sin\theta\sin\psi & -\sin\phi\cos\psi + \cos\phi\sin\theta\sin\psi \\ -\sin\theta & \sin\phi\cos\theta & \cos\phi\cos\theta \end{pmatrix}$$

Here we purposely avoid using Euler angles to express rotation matrix to solve the problem for the following two reasons. First, P^0 and P^1 in this case will not necessarily be from the same sensor due to remote sensor usage (the sensor might be misoriented for all the data from this sensor). Within the sensor, there is inherent noise due to MEMS technology and the noise distributions from different sensors are not independent and identically distributed. So if we take P^0 from a different sensor, we need to model the noise, which makes the problem very complicated. Second, the computation will involve trigonometric function and computational complicated.

An alternative is to convert the above problem into a neat optimization problem as expressed in equation 3.11 It's called orthogonal procrustes problem [Gower and Dijksterhuis, 2004] and has been solved by Peter Schonemann in 1964. The solution to R is shown in equations 3.12 to 3.14.

$$R = \arg\min_{\Omega} \parallel A\Omega - B \parallel_F \text{ s.t. } \Omega^T\Omega = I \tag{3.11}$$

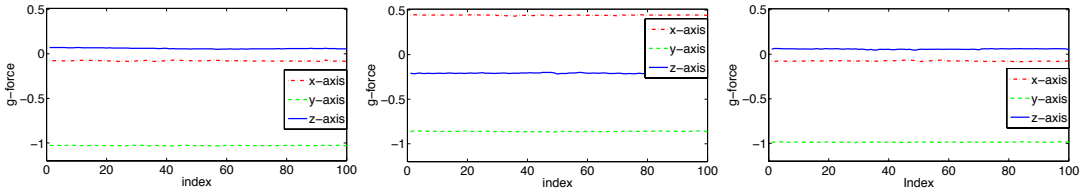

(a) P^0 from an appropriately mounted sensor (b) P^1 from a misoriented sensor (c) Orientation corrected P^1

Figure 3.10: Visualization of P^0, P^1 and corrected P^1

$$M = P^{0T} * P^1 \tag{3.12}$$

$$(U, D, V) = \text{SVD}(M) \tag{3.13}$$

$$R = U * V^T \tag{3.14}$$

In order to get the rotation matrix R, P^0 in this case is a vector of 100*3 from a different sensor that is in sedentary state and P^1 is a vector of same length from the misoriented sensor in sedentary state. Figure 3.10 visualizes the P^0 and P^1 vectors as well as the corrected P^1 vector. Figure 3.11 shows and example of orientation corrected data from an episode of walking event and peak detection result before and after sensor orientation correction.

3.4.3 Speed, Stride Length, Cadence, Traversed Distance Modeling

3.4.3.1 Speed Modeling

The most critical component of kinematic modeling is to develop a *speed* estimation model, since it is the basis of computing the other parameters.

During training, the subject is instructed to walk three different walking speeds for a known and fixed length of distance. A speed vector $V = [V_{avg}, V_{fast}, V_{slow}]$ could be derived by $v = s/t$, where s (distance, equal to 50 feet) and t (time) are known

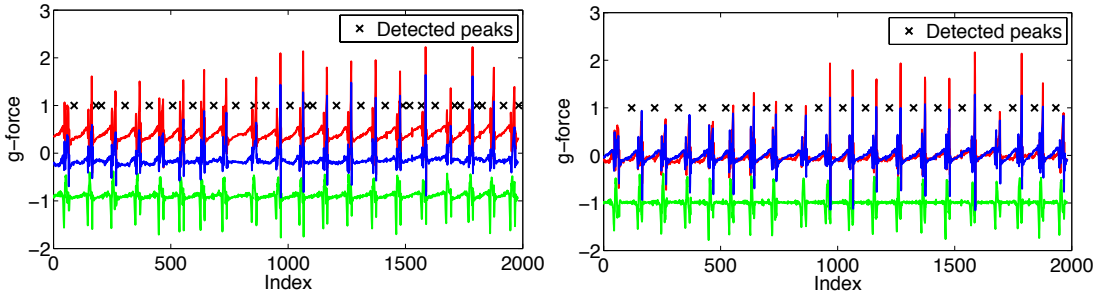

(a) Before sensor orientation, with an accuracy of 71.43%

(b) After sensor orientation, with an accuracy of 100%

Figure 3.11: Sensor data reorientation and peak detection result, with peaks shifted half a phase

parameters. A time vector $t = [t_{avg}, t_{fast}, t_{slow}]$ is also derived from the walking sections, where t is the walking cycle period as shown in figure 3.8. A linear relationship is hypothesized to exist between these two vectors and least squares method is applied to derive the parameter set $[p1, p2]$. Given a new set of walking sections a step to step speed (m/s) can be calculated as shown in equation 3.15, where t is walking cycle period calculated from the raw data by peak detection.

$$\text{Speed} = p1 \times td + p2 \tag{3.15}$$

3.4.3.2 Stride Length, Cadence, Traversed Distance Modeling

Cadence is naturally reversely proportional to the walking cycle period t in figure 3.8. Cadence is defined in equation 3.16 with a unit of steps per second. It count a sum-up strides from both limbs.

$$\text{Cadence} = \frac{2 \times 60}{t(i)} \tag{3.16}$$

Stride length(in meters) is defined as the distance traversed in a complete walking cycle defined in figure 3.8 by one leg. Equal stride length is assumed unless the sub-

ject is turning around. Since turning only affects one or two steps this condition can typically be ignored. Thus, equation 3.17 is derived as follows.

$$\text{Stride Length} = \frac{\text{Speed} \times 120}{\text{Cadence}} \tag{3.17}$$

Finally, combining equations 3.15 to 3.17, distance traversed can be expressed as equation 3.18, where n represents the number of strides performed by one leg.

$$\text{Distance} = \sum_{i=1}^{n} \text{stridelength} = \sum_{i=1}^{n} (p1 \times t(i) + p2) \times t(i) \tag{3.18}$$

3.4.4 Kinematic Parameters Validation

A blind test was conducted to validate the kinematic parameters modeling. Dr. Bruce Dobkin from neurology department of UCLA instructed 6 stroke patients to walk a distance and conceal the length. Figure 3.12 shows the groundtruth and the calculation. The averaged error rate is within 10% and meets clinical need. Table 3.2 shows the detailed statistics. Furthermore, in the data for single trip experiments, extra steps outside the route boundary are possible and cannot be ruled out by the automated algorithm, which contributes significantly to the error. For a double trip, the effect of outside steps is attenuated due to the longer distance. Dr. Dobkin pointed out in [Dobkin et al., 2011a] that "A high correlation was found between stopwatch-measured outdoor walking speed and algorithm-calculated speed (Pearson coefficient, 0.98; P=0.001)".

3.5 SIRRACT: Stroke Inpatient Rehabilitation Reinforcement of Activity: An international MRCT Network

3.5.1 Introduction

SIRRACT is an international, multi-site, randomized controlled study with blinded outcome measures. There are more than 13 sites, distributed in 11 countries and districts,

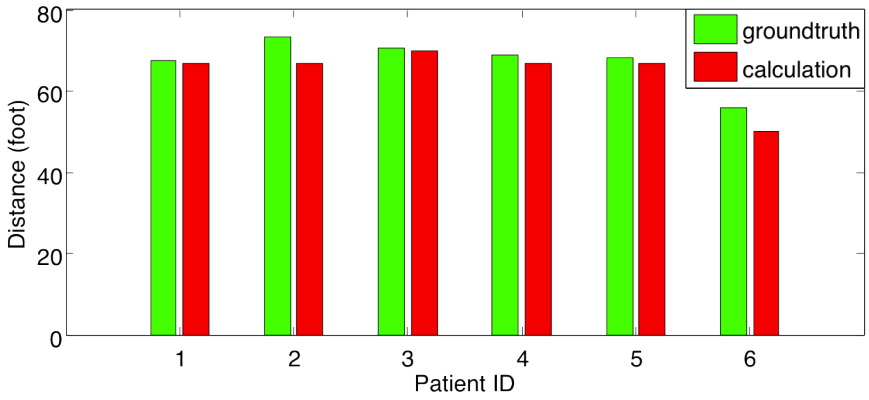

Figure 3.12: Blind test visualization. It comapres performance of speed calculation with groundtruth recorded by Dr. Dobkin

Table 3.2: Speed Validation Statistics

Subject Number	A toB(ft)	B to A(ft)	Round Trip(ft)	GT(ft)	Error Rate for Single%	Error Rate for Round Trip%
NO.1	67.51	81.75		66.35	11.83	
NO.2	73.24	80.51	150.7	66.35	15.20	12.89
NO.3	68.60	70.64		70	1.457	
NO.4	57.59	63.18	112.1	50	5.966	1.643
NO.5	74.71	68.74	121.6	66.75	7.480	8.918
NO.6	68.32	78.50	137.60	66.75	10.00	3.100

Figure 3.13: SIRRACT sites global distribution

and more than 150 patients are involved. Figure 3.13 shows the global distribution of SIRRACT sites. Subjects, who are mainly stroke patients accepting physical therapy in rehabilitation unit, wear the motion sensors during their day time. The site manager uploads data to UCLA WHI server (labeled as red start in figure 3.13) through a software called MDAWN uploader. The system on UCLA WHI server will classify the activity and provide feedback to site managers with kinematic information summaries. Currently, the activity of concern is gait.

3.5.2 Running of SIRRACT

3.5.2.1 The hardware

The motion sensors used in SIRRACT is referred as Medical Daily Activity Wireless Network (MDAWN) devices, shown on figure 3.14a. The sensing devices are manufactured by Gulf Coast Data Concepts(GCDC) [mda]. The MDAWN sensing platform contains a three-axis accelerometer that can be tuned to record motion with magnitudes

up to 6g on each axis. The devices operate in logging mode, storing the data on an internal SD card. The sampling rate of the MDAWN devices can be selected anywhere in the range from 10Hz to 320 Hz. The sampling rate of 40Hz was selected for the presented experiments according with findings from [Bouten et al., 1997], stating that the frequency of human behavior caused by voluntary muscular work is under 20 Hz. Therefore, the selected sampling rate satisfies the Nyquist criterion. The devices have a capability to maintain accurate clock, which enables timestamping of the archived data. Finally, the devices use a USB interface for data upload, operation parameter modification and charging. The on board rechargeable battery lasts 48 hours under continuous sampling with the parameter setup used in our experiment.

Figure 3.14b shows a complete kit for deployment, consisting of a sensing platform and a flexible attachment band that can be conveniently used to mount the system around wrists or ankles. Velcro is used to attach the sensing platform to the flexible band. The sensing module is mounted on ankles of subjects in the experiments presented in this paper, since the focus is on the walking activity characterization. The system is nonintrusive due to the light weight (2 sensors and 2 bands weigh less than 50g in total) and small size of the device (comparable to a conventional USB flash drive). As mentioned above, the MDAWN devices can be charged via the same USB interface. During long term deployment campaigns, the MDAWN kits also include USB hubs and AC power adapters to enable simultaneous recharge of multiple devices from a computer or an AC wall outlet. Therefore, the described kit can operate for periods of over two weeks without technical intervention, which is convenient for home environment usage and most applications.

3.5.2.2 Data Upload

Collected motion data is archived on on-board SD card. When data needs to be uploaded, MDAWN is plugged into the USB port of a computer and a software called

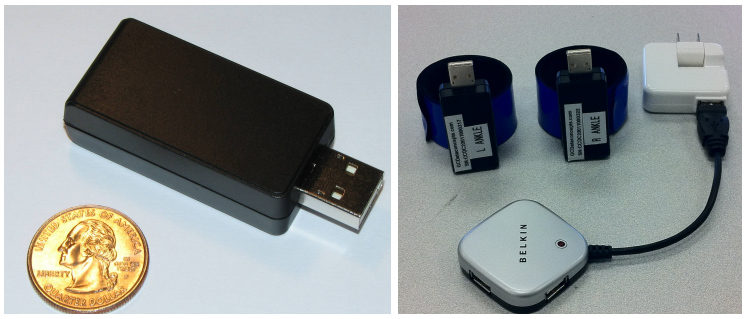

(a) MDAWN platform (b) Complete kit

Figure 3.14: Hardware platform and deployment kit in SIRRACT

"MDAWN uploader" is started. The destination of upload is hard coded as the UCLA Wireless Health Institute server eawins38.

Figure 3.15 shows the user interface of the software. When "Discover" button is pressed, the software will begin to search for connected MDAWNs from USB port. When "Upload" button is pressed, the software will upload data files in each MDAWN chronologically using SSH protocol. When "Sync" button is pressed, the software will write the current time on the computer to the internal clocks of connected MDAWNs. In other words, the clock of connected MDAWNs are synchronized. When "Close" button is pressed, the software will exit.

3.5.2.3 The Procedure

The signal processing system of SIRRACT includes two steps, the automated training and automated post processing. Figure 3.16 a shows the flowchart of training step and figure 3.16 b shows the flowchart of postprocessing step.

In training module, the data is first analyzed by the preprocessing module. During this stage it is important to ensure that the data from multiple sensor devices is aligned in time, represents the same or known sensor orientation (so that the data can be interpreted in a similar manner) and has identical spatiotemporal resolution. Therefore, the

Figure 3.15: MDAWN uploader interface

data files are merged according to the timestamp and any non-continous regions in the merged data, which is accomplished by shifting the data points to the correct positions within identical temporal windows and interpolating data whenever necessary. In this paper the system assumes that there is no significant location or orientation uncertainty in the sensor placement.

For the training data collection procedure, each subject is asked to walk a marked distance of 50 feet with the speeds of ”average”, ”slow” and ”fast” - as perceived by the subject. Please notice the limited amount of training data required (only 3 bouts of 50 feet walking). Furthermore, note that the three different speeds are controlled completely by the subject and do not have to be similar among all of the subjects. The rationale for requiring three different speeds is to obtain gait variability characteristics and capture corresponding templates in training data. In order to further automate the training data collection process, a start and an end signatures are attached to each walking section. A signature recognition algorithm is applied to delimit each walking section, avoiding the tedious manual noting effort. The ”Start” signature consists of

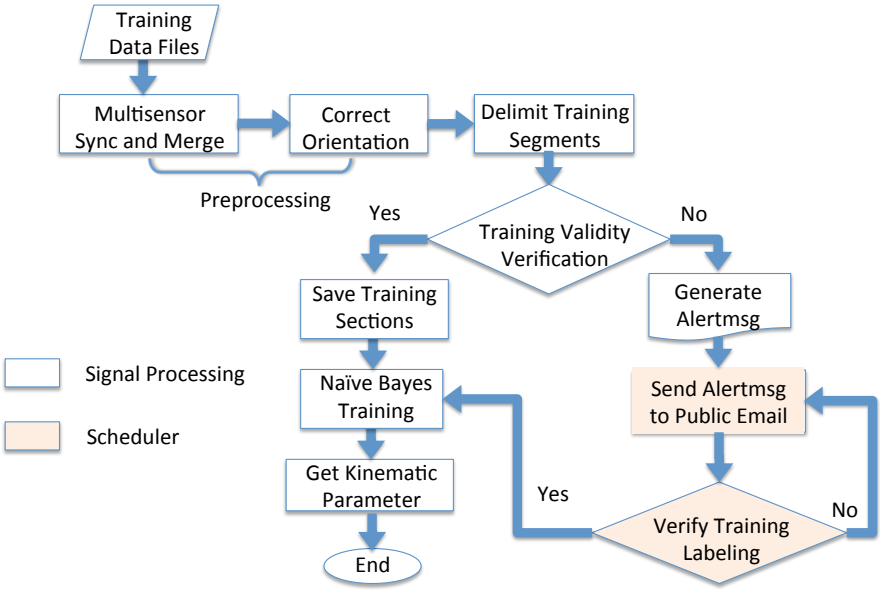

(a) Training flowchart

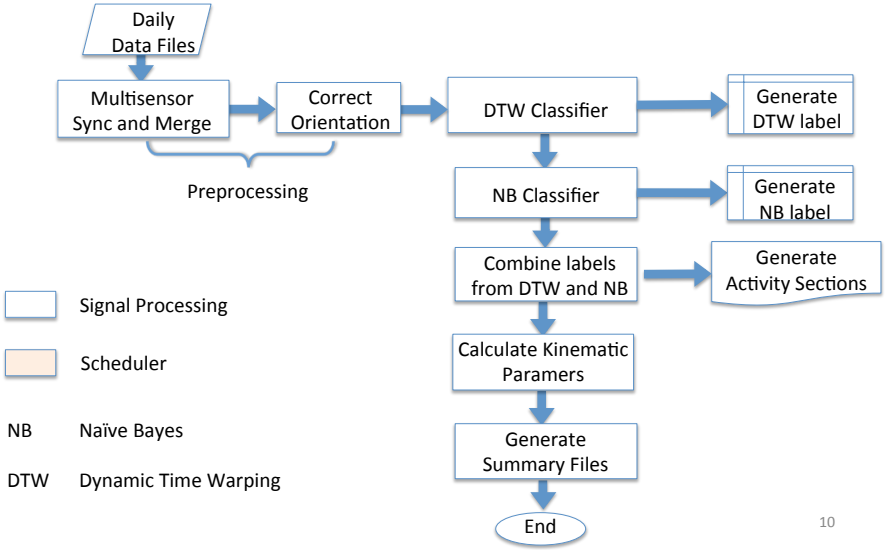

(b) Post processing flowchart

Figure 3.16: Signal processing system in SIRRACT

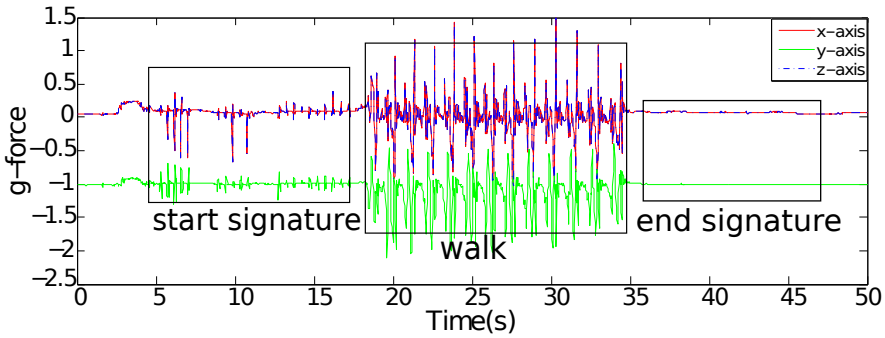

Figure 3.17: A standard walking section. It has a start signature of 5-5-10 tappings with 1 second separated, and an end signature of being static more than 10 seconds

tapping the sensor with a predetermined sequence (e.g. five-five-ten times). The ”End” signature consists of at least 10 seconds of relative immobility. This is performed by simply requesting the subject to stay stationary for 10 seconds at the end of every training episode. Fig.3.17 shows an example of the standard walking section with a ”start” and an ”end” signatures. The DTW algorithm is employed to match the start signature with a pre-saved template. The signature detection algorithm is applied separately on the data from all three axis of the motion sensor and the returned results are compared with an empirical value. In practice the developed signature detection algorithm is remarkably robust including the cases when the ”tapping” template is recorded by a different user. In cases when the automated system recognizes a different number of training episodes than those declared to the system by the user, a manual intervention is required. Note that this limited training needs to be performed periodically. Currently, it is required to do training on a weekly basis.

Figure 3.18 shows the training procedure.

Post processing module is executed whenever the data marked as testing is uploaded into the server. The data passes through the same preprocessing modules as in the training module. It next goes through a hybrid classification system to classify motion of interest. After episodes of motion have been identified, it calculates kinematic infor-

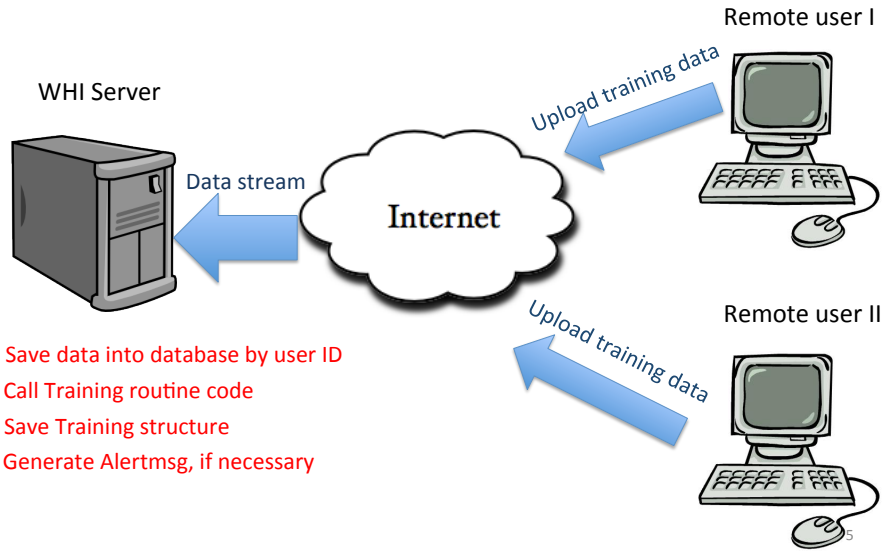

Figure 3.18: Training procedure

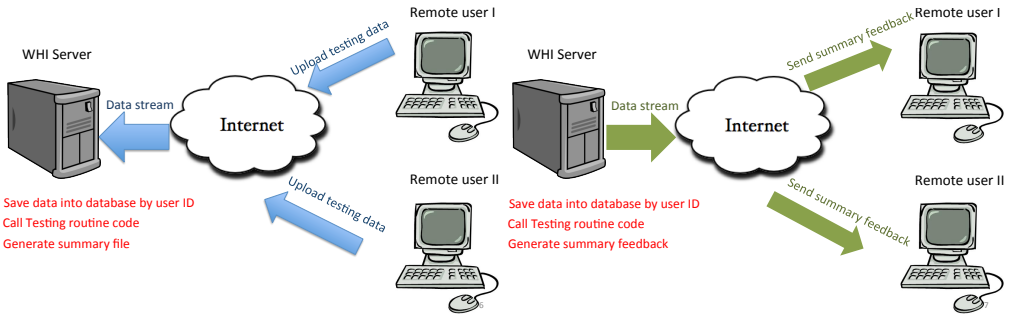

Figure 3.19: Post processing procedure

mation and generates summaries, which will be distributed to individual site.

Figure 3.19 shows the post processing procedure.

3.5.3 Large-scale Data Management System

The medical data entry system for SIRRACT is located at `https://www.npistat.org/sirract/Login.asp`. Each site has their own account on the data entry system. When a new patient is enrolled into SIRRACT study, the site manager will register this patient with a new patient ID, record the demographic information and assign two

MDAWNs to this patient ID . When the patient finishes the study, the site manager will unregister this patient as well as the MDAWNs. The MDAWNs then can rotate for other patient usage.

Due to IRB approval issues, the SIRRACT data entry system webpage is not hosted by the UCLA Wireless Health Institute engineering team. However, we host a replicate data management system that will sync data with the medical database every 10 minutes. The scheduler on UCLA WHI server will call the routine code for SIRRACT when new data found.

3.5.4 Deployment, Lessons and Experience

We assign 3 sets of MDAWN pairs to each site for patient rotation and device replacement. We keep the convention that the device's serial number ending with odd is labeled as "left" and ending with even is labeled as "right". The package we mail to each site includes 6 MDAWNs, 3 labeled as left and 3 labeled as right; one 10-port powered USB hub; 6 reflexive bands; extra velcros for position adjustment as well as a printout of "MDAWN Upload and Maintenance Protocol" which specifies the basic steps of data upload. For certain sites, we also mail a netbook with Windows7 installed to facilitate data upload.

During running of SIRRACT, we noticed problems from IT systems, data upload, sensor usage, outcome measure, classification performance, etc.

In IT system, we noticed the following problems

- The firewall of medical network has strict restrictions on data transport. We have to talk to their IT people to allow SIRRACT data upload.
- The international network is unstable in some countries. We have to manually retrieve data through file hosting service, such as dropbox.

- The MDAWN devices can not be discovered by the uploader, which results in data loss. There are a couple of possible reasons, such as broken devices, operating system compatibility (currently Windows OS is supported), USB ports are occupied by OS at the time, etc. We specify a bunch of solutions in "MDAWN Upload and Maintenance Protocol" such as unplug the USB hub and plug in again.

During data upload and sensor usage, we noticed the following problems.

- The start and end signal of signature in training is not executed properly.

  People may tap on both sensors as a start signal, or wait a very long time between tapping and walking, or there is no ending signal at all. We now have to disable this function and turn into total manual delimitation for training.

- The devices are not synced properly.

  Clocks in MDAWNs will drift overtime and make the motion data from left and right ankles misaligned. We require the site managers to "Sync" sensors when uploading data on a daily basis. The "Sync" button of the uploader is neglected to be pressed frequently. Figure 3.20 shows two examples of clock drift. The misalignment in figure 3.20 a makes the alternating activity of gait into a simultaneous movement. In figure 3.20 b, the clock drift is so severe that there is no common sections from the two sensors and makes the movement uncorrelated.

  This problem needs manual inspection and manual correction.

- The devices are not orientated properly on ankles.

  The current system automatedly detects up-side down orientation issue since initially we believe the other misorientation problem is hard to happen due to sensor attachment method in figure 3.14. However, in reality problem such as figure 3.11

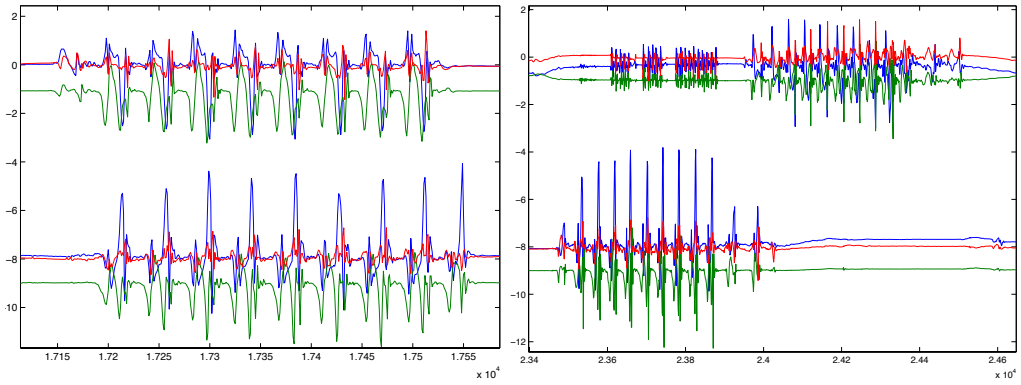

(a) Simultaneous Strides (b) Non Correlated Strides

Figure 3.20: Data misalignment examples

happened. This problem is detected manually and corrected using method introduced in section 3.4.2.

- The sensor is used in wrong position.

  For example, the sensors used on left ankle and right ankle are switched or sensor used for one patient is mistakenly used for another. This problem is very hard to detect as well. For the first issue, it can be manually inspected if x axis and z axis are in phase or out of phase. According to figure 3.8, x and z axes on left ankle are out of phase while on right ankle are in phase. For the second issue, motion correlation can be checked.

- The sensors are deleted from the system instead of being unregistered.

  The negligence of deleting SN of sensors from the database system breaks the link between raw data and patient ID. Data retrieval is impossible. The valuable motion data of particular subject is immersed in raw data files that is only referenced by serial number.

I access the medical database of SIRRACT to get ground truth information for data processing. The following issues about outcome measure are observed

- The rehabilitation scales are not recorded properly.

  For example, in one site, the patients' FAC level at admission is 5, the highest, and has various values which is below 5 when discharged. This issue happens for more than half of patients on that site. The site admitted it was their error. However the experiment is inconvenient to reproduce and the valuable groundtruth information is lost.

- The stop-watch recorded time length has a hard coded upper limit in the medical database.

  The upper limit is 140 seconds. However for very weak patients, the 50ft walk can be beyond this limit. The nurse can only input 140s in the medical database which is misleading.

The classification suffers from both type I error (false positive) and type II error (false negatives). Figure 3.21 shows the example of false positives and false negatives.

In figure 3.21 a, it is observed that 16 seconds of gait (from 24874 to 24890) that has been misclassified. The feature distribution falls into the training data's distribution of patient. This episode corresponds to the end of day and it is hypothesized that this motion comes from the situation that the physician takes the sensor away from the patient and carry them back to office. The data is simultaneous if observed carefully, thus there is high correlation among certain axes. I make use of this property to eliminate similar sections.

In figure 3.21 b, a 10 seconds episode (from 3390 to 3400) is labeled as not being gait. The transitional gait section as shown in this example is usually ignored by the algorithm due to the fact that feature value among this section doesn't fall into the training feature distribution (notice the gaps within this section). This is no good solution based on the current algorithm, however, promising solutions proposed in chapter 5, which makes use of gait pattern. It's not as sensitive to the noncontinuous gait episode

as the algorithm proposed in this chapter.

3.6 Discussion

Applications of low cost energy efficient technology and machine learning techniques to monitoring and characterizing human activity and behavior will be critical in enabling many new systems that can improve the quality and breadth of delivery of healthcare, reduce healthcare costs by encouraging adherence to activity regimen providing disease prevention methods. In order to meet the demands of these new applications, however, human motion analysis should become automated, validated in community trials and applied in free-living community conditions. These requirements are critical because 1) There is a profound difference between human motion analysis in the laboratory and in the community and between normal subjects and patients with afflictions and 2) There is a unique opportunity today to make a difference in the lives of many patients seeking any help available in recovering from the diseases where activity monitoring and promotion can undoubtedly make a difference.

This chapter presents a novel hybrid approach for human motion activity classification. This approach is based on a multitiered combination of the Naive Bayes classifier and the Dynamic Time Warping algorithm. In the approach presented in this chapter, the outputs from the two algorithms are combined in such a way as to retain the high confidence in the final classification result, while segmenting a large correctly identified classification set.

This chapter also presented an approach for speed estimation in the classified "walking" segments. It is important to note that some of the other gait parameters (cadence, step length, swing ratio) can be computed from the speed estimate directly or using similar analytical approaches.

In this chapter we have presented results from a group of 6 subjects engaged in

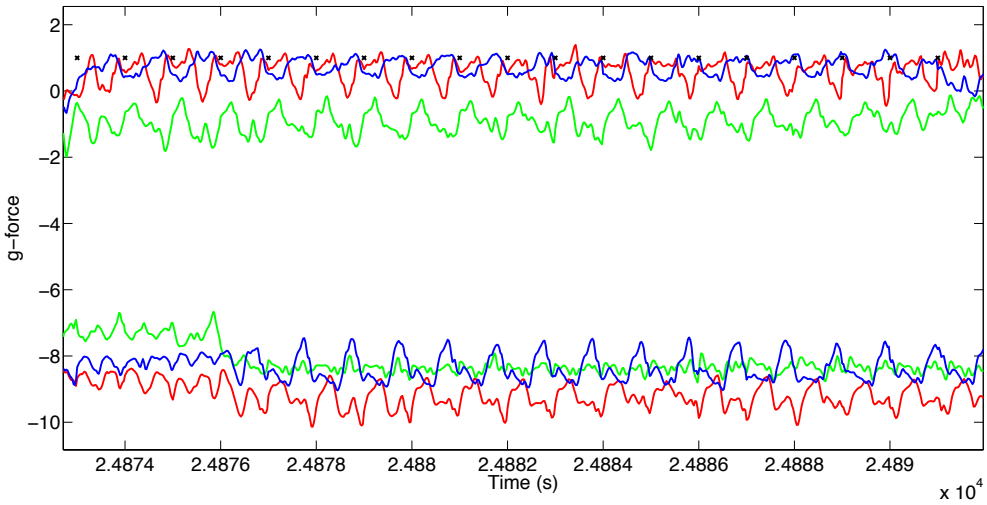

(a) False positive example

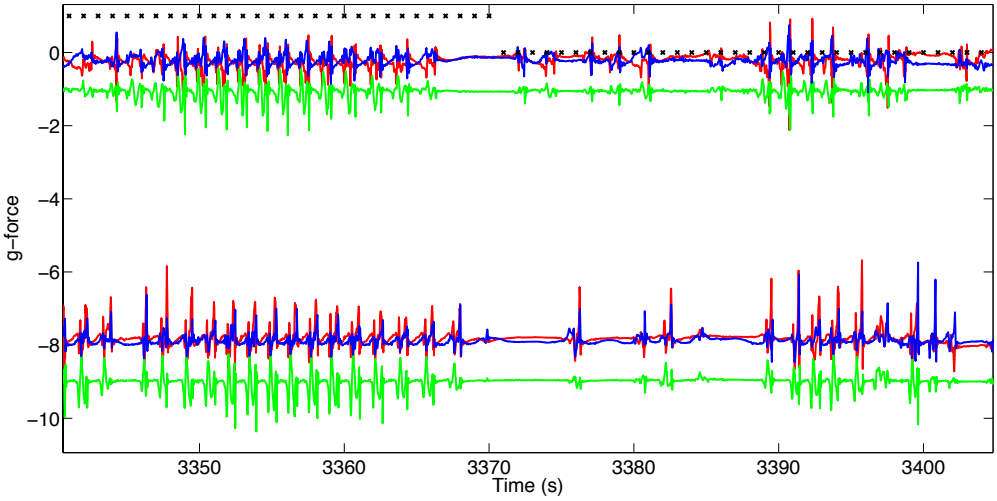

(b) False negative example

Figure 3.21: False positive and false negative example in classification of SIRRACT study. The black cross represents classification result in seconds; the upper part is from left ankle and lower is from right ankle; the upper and lower and 8g separated to avoid plot overlapping; rgb correspond to x y z axis.

formal trials through neurological rehabilitation, exhibiting hemiparetic walking gait. The focus of the motion analysis was on the walking activity segmentation and characterization. The hierarchical approach clearly outperformed a purely Dynamic Time Warping or Naive Bayes approach and shows the benefits of the layered design. Finally, the speed computation was verified to be accurate (on average to within 10%).

This chapter extends capabilities of the algorithms presented in this chapter to serve large communities and an expanded set of disorder conditions, the international, multi-site study, SIRRACT. Detailed techniques such as motion sensing hardware, signal processing system routine, data upload software and large scale data management system are also introduced. We summarize the experience and lessons from SIRRACT. We believe this is valuable for future large scale trials.

The future work is to employ methods to discover the internal structure of the diversified data. It will not require personalized training structure and will be more convenient to deploy.

CHAPTER 4

Visualization: A Longitudinal Analysis

4.1 Introduction

The conventional assessment methods of post-stroke patients' motor functions are conducted through standard scale tests [str]. Such tests require patients to perform different tasks typical for every-day motions when in the community. The performance of patients is then scored by a physician or a qualified personnel. These tests and methods, however, suffer from the subjectiveness of physician's judgement, minor changes in specifics of the task performance or conditions in which the test is conducted.

The low-cost wearable sensing devices are prosperously developing and being deployed in a variety of healthcare monitoring and assessment applications [Xu et al., 2011]. Wearable sensor monitoring have shown to be complementary for performance evaluation and can be deployed for monitoring in the community with feedback provided to the physicians and patients on a daily basis [Xu et al., 2011; Wang et al., 2011].

In this chapter, algorithms for detailed analysis of the motion (e.g. accelerometer) data are presented, where variations in each stride of the subject during locomotion are analyzed, providing a quantitative and qualitative description of post-stroke patient's walking. This paper has the following contributions: Firstly, an on-line methodology for computing clinically relevant metrics and characteristics for subject lower body mobility. Secondly, a metric vector, purely derived from the accelerometer data and independent of sensor orientation. Thirdly, a visualization method that indicates motion

quality evolution during and after patient rehabilitation based on a longitudinal data. This enables physicians, patients and other interested parties to visualize the effects of the rehabilitation and treatment.

4.2 The Evaluation Metric: A Quality Vector

The motion quality evaluation metric includes kinetic characteristics and motion variability. These metrics are independent of the orientation around the ankle placement given an ankle band mounting method described in [Xu et al., 2011] and are feasible for large scale experiment deployment. The hardware is an energy efficient platform with tri-axial accelerometers [mda].

4.2.1 Kinematic Characteristics

Kinetic characteristics include walking speed, cadence, stride length, symmetry and swing to stride ratio (SSR). Modeling of speed, cadence and stride length has been elaborated in [Xu et al., 2011].

Symmetry is defined as a ratio of the impaired leg swing time over the normal leg swing time [Patterson et al., 2010]. Figure 3.8 shows a stride segmentation from two legs. SSR is defined as a ratio of the swing time over the complete walking cycle period t shown in figure 3.8, which is a sum of swing and stance times.

The walking cycle is identified by a peak detection algorithm, which has been elaborated in section 3.4.1.

4.2.1.1 Stride Segmentation: An Adaptive Swing Matching

Within a stride that contains a complete swing phase, an adaptive matching algorithm is applied to precisely identify its location.

This algorithm first performs a search within the stride data S through all of its sub strings to identify the one that has the smallest distance compared to the template, shown in Eq.4.1. substring$^-$ represents the initial match result. The distance metric is calculated by the Dynamic Time Warping [Sakoe and Chiba, 1978]. This provides an estimate of the similarity between the stride substring and template. Motion data signal warping caused by different walking speeds are adjusted accordingly.

Next, substring$^-$ is extended and shrank on both ends of the boundary indices and the distance array is searched to find the minimal distance. The corresponding substring is the final match.

$$\text{substring}^- = \arg\min(\text{Dist}(\text{stride}, \text{template})) \tag{4.1}$$

$$\text{substring} = \min(\text{Dist}, \text{Dist}_{shrink}, \text{Dist}_{expand}) \tag{4.2}$$

Algorithm 2 shows the process. The input is a data vector of a stride and a swing phase template, that has been precomputed. Lines 1-7 show the initial matching process. $startind$ and $endind$ in algorithm 2 are the start and end indices of the initial match.

Lines 8-17 show the adaptive searching part of the algorithm, where lines 8-12 and lines 13-17 expand and shrink the sub string length of stride S separately. Finally, line 18 finds the minimum distance of the three distance vectors and line 19 obtains the proper swing length by adjusting the $startind$ and $endind$. Figure 4.1 shows an example of expanded matching.

4.2.2 Variability

Variability is an important qualitative measurement of stroke patients' walking functionality [Oken et al., 2008]. We define an entropy parameter to characterize variability and randomness in the walking data.

Algorithm 3 shows the process to calculate entropy. Input is a vector of stride

Algorithm 2 Adaptive Swing Phase Matching

Data: $s, template$

Result: $swinglen$

begin

  for $n = 1 : len(s) - len + 1$ **do**

    $d(n) = dtw(s(n : n + len - 1), template)$

  $ind = find \min(d)$ $startind = ind + 1$ $endind = startind + len(template) - 1$ $start_{expand} = startind - 5 > 0 ? startind : 1$ $end_{expand} = endind + 5 < len(s) ? endind + 5 : len(s)$ **for** $n \in [start_{expand} : end_{expand}$ **do**

    $d_{expand} = dtw(s(n), template)$

  $start_{shrink} = startind + 5$ $end_{shrink} = endind - 5$ **for** $n \in [start_{shrink} : end_{shrink}$ **do**

    $d_{shrink} = dtw(s(n), template)$

  $shiftind = find \min(d, d_{shink}, d_{expand})$ adjust $startind$ and $endind$ with $shiftind$ return $swinglen$

end

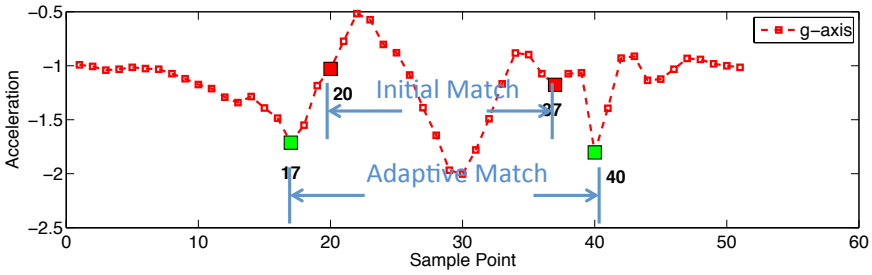

Figure 4.1: Swing phase adaptive matching

signals and a threshold value. The stride signals are automatedly delimited by method proposed in 3.4.1. The output of the algorithm is the entropy value. In algorithm 3 lines 1-7 generate a lower-triangle distance matrix of the stride vector, that is, a distance matrix for every two strides. Each item in the distance matrix is a measurement of signal similarity between the two strides.

The distance matrix is then compared against the input threshold. The input threshold is determined by the mean value of the distance matrix precomputed from a population of the healthy subjects. The algorithm then clusters the strides by their mutual distance. That is, if $D(i, j) < threshold$, then stride i and stride j are defined as linked and thus merged into the same cluster. Lines 11-14 show this process. The algorithm stops looping when the number of clusters does not change.

After this step, the strides are merged into different clusters on the basis of their similarity. Finally, the entropy value is calculated according to the definition. The entropy is upper bounded by $\sum \frac{\log n}{n}$ and lower bounded by 0.

Figure 4.3 shows the link and merge example. The threshold in this example is 5. After link and the initial step of merge, 17 clusters are generated. They are $\{1, 3, 5, 6, 7, 8, 9, 10, 11, 12, 13, 15, 17, 18\}$, $\{2, 5, 9, 18\}$, $\{3, 7, 8, 9, 10, 15\}$, $\{4, 5, 9, 10, 15\}$, $\{5, 7, 8, 9, 11, 13, 14, 15, 17, 18\}$, $\{6, 8, 9, 10, 12, 13, 17\}$, $\{7, 8, 9, 11, 13, 14, 15, 18\}$, $\{8, 9, 10, 11, 12, 13, 15, 17\}$, $\{9, 10, 11, 12, 13, 15, 17, 18\}$, $\{10, 11, 12, 13, 15, 17, 18\}$, $\{11, 13, 14, 15, 17, 18\}$, $\{12, 17\}$, $\{13, 14, 15, 17, 18\}$, $\{14, 15, 17, 18\}$, $\{15, 17, 18\}$, $\{16\}$, $\{17, 18\}$. The merge step is repeated iteratively until the number of clusters becomes stable. In this example, the final clusters are $\{1, 2, 3, 4, 5, 6, 7, 8, 9, 10, 11, 12, 13, 14, 15, 17, 18\}$ and $\{16\}$. And the entropy value is calculated as 0.2146. From this calculation, stride 16 is an outlier which is different from others. Raw data evidence is shown in figure 4.2. The circled stride is 16. The profile of this stride is clearly distinct from others.

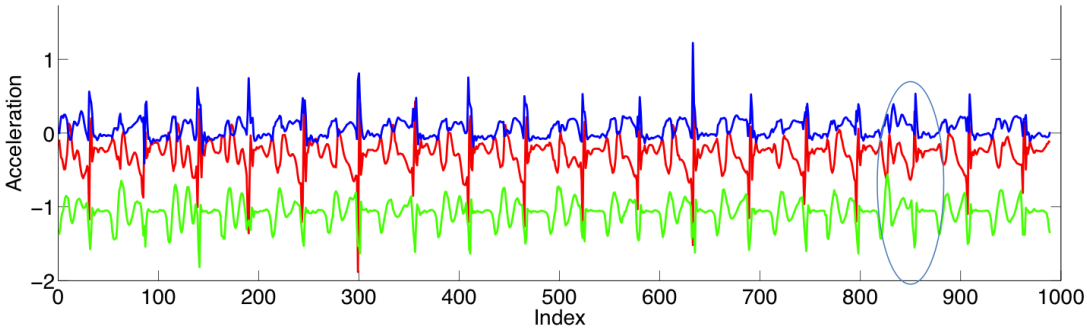

Figure 4.2: Raw data evidence for variability

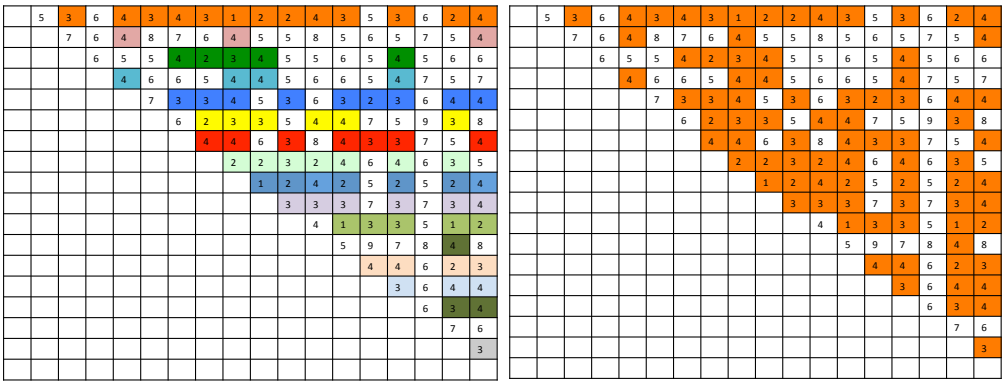

(a) Link (b) Merge

Figure 4.3: Link step and merge step

Algorithm 3 Entropy Calculation

Data: $S = (s_1, s_2..., s_i, ...s_j)$,$threshold$

Result: $Eval$

begin

  for $n = 1 : j$ **do**

    for $m = 1 : j$ **do**

      if $m \geq n$ **then** continue **else** $Dist(n, m) = dtw(s_n, s_m)$

  for *n=1:j* **do**

    $index\{n\}$=find $Dist(n, :) < threshold$

  for $index\{i\} \in index\{1 : n\}$ **do**

    if $index\{i\}\&index\{j\}! = 0$ **then** merge index{i} and index{j}

  for $n = 1 : len(merg\_cluster)$ **do**

    $prob(n) = len(merg\_cluster(n))./len(S)$

  $Eval = -1 * sum(prob. * log(prob))$

end

4.3 Experiments

For the experimental evaluation of the proposed algorithms, 20 subjects have been recruited. Nine of these subjects are healthy individuals with subject IDs 1-9, and the other 11 are stroke patients with different severity of the condition and IDs of 11 to 17. An appropriate UCLA IRB and the subject consent approvals were obtained before the experiments. Of the 11 stroke patients, seven have records for only one time evaluation and the other four have longitudinal records including evaluations of four and more times over the period of several weeks. Those four patients are participants of the SIRRACT [sir] project (with IDs 17 to 20). The experimental data includes 36 unique data records and observations in total.

Each subject was instrumented with two tri-axial accelerometer devices referred as MDAWN [mda], one around each ankle. Both MDAWNs of every patient are time synchronized before the data collection and monitoring. Each subject is instructed by the physician to walk with three different speeds (fast, average and slow) moderated by the subjects themselves, traversing a distance of 33 to 50 feet.

The complete metric vector includes $entropy_{left}$, $entropy_{right}$, $symmetry$, SSR_{left}, SSR_{right}, $speed$, $cadence$ and $stridelen$, and is calculated for each subject. The kinetic parameters are averaged during the test.

A matrix of 36 by 8 is generated (e.g. number of observations vs metric vector). In order to provide effective visualization of the recovery evolution for these patients, the matrix is subjected to the principal component analysis (PCA). Eight principle components are generated and the first two explain 84.78% of the variance. The algorithm then projects the observations onto the first two dominant principle components for the data from the four longitudinal patients, as shown in Fig.4.4.

The green stars in the Figure represent the data cluster for the nine healthy subjects. The red crosses represent the seven stroke patients that have only one-time record, and

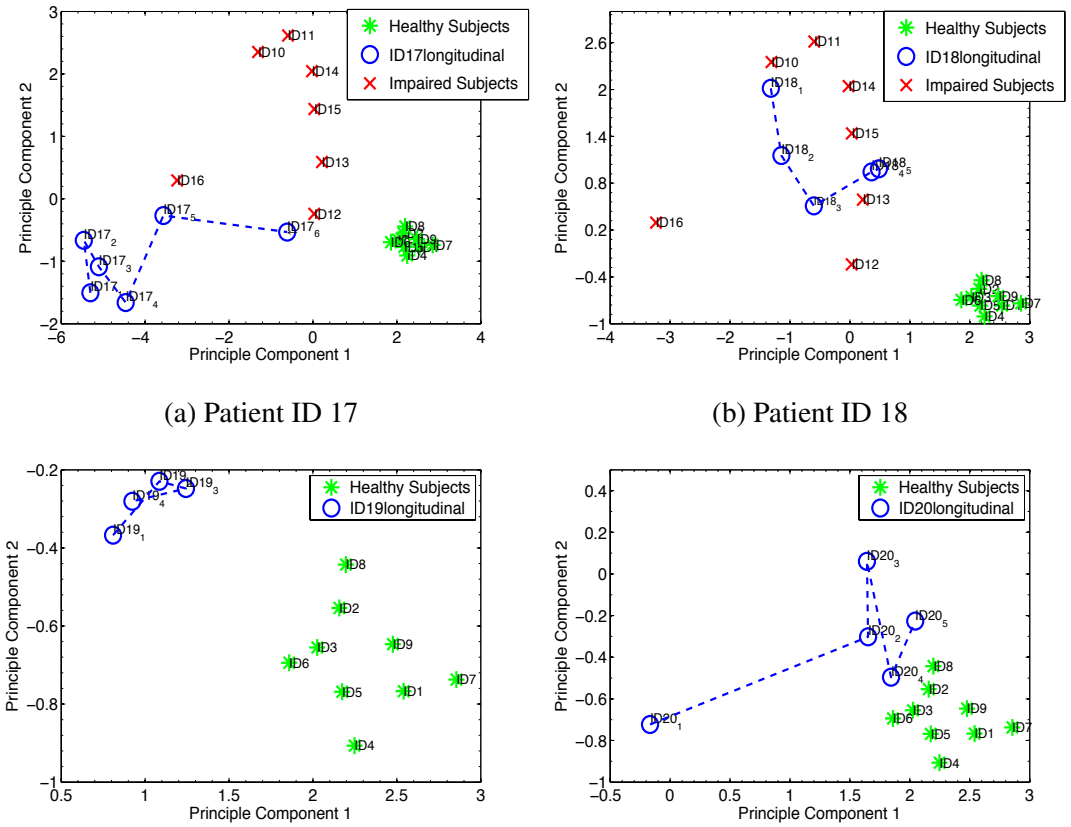

(a) Patient ID 17

(b) Patient ID 18

(c) Patient ID 19

(d) Patient ID 20

Figure 4.4: Patient gait evolution visualization

the corresponding cluster. These are the two control groups. The linked blue circles in each figure (referred as anchor points in this thesis) represent the evolution route of the individual patients from the moment they are first admitted to the hospital until discharge with comparison to the control group data overlaid.

Figure 4.4a-d have different resolutions according to the performance of the patient. Patient ID17 and 18 are generally weaker, while patients ID19 and ID20 have better performance initially. Thus, in the last two subfigures, the control group of the nine stroke patients is not shown. In these cases the goal is to emphasize the distance between the healthy control group and the patient recovery evolution route.

4.4 Discussion

In this chapter, we explore the methods to derive metrics of variability, swing ratio, swing stance time, speed, stride length and cadence from pure accelerometer data, and decompose the signal to visualize the evolution process of patient recovery.

This method is not limited to stroke patients. It can be applied to other communities, such as patients with Parkinson's or Multiple Sclerosis conditions. The metric value itself provides a physician with the relevant information about the patient on a frequent time basis (for example daily), and can alarm when abnormal events occur. Furthermore, some of the metrics, for example entropy, can provide physician with prognostic inference about a likely fall.

The visualization provides macroscopic view of the patient performance over a longer period of time and can aid physicians to better understand recovery process.

The visualization also provides clustering based on the performance of the patients. However, with limited observations, it is too early to draw conclusions. In the near future, with more patients recruited to the SIRRACT [sir] project, the project is on its way towards data analysis for a larger group of stroke patients. Besides, during the evolution path, certain anchor points might represent pathological conditions. That is, the patient is not marching towards expectation in a desirable way. It needs to be inspected.

Currently the metrics employed in this chapter are all from motion sensors. It will be valuable to combine the motion sensing metrics with physician evaluation scales and derive a scoring system that will be applied to gait quality evaluation.

CHAPTER 5

Scaling for Big Data

5.1 Introduction

Scalability is defined as the the ability of a system, network, or process, to handle growing amount of work in a capable manner or its ability to be enlarged to accommodate that growth. However, following challenges are emerging associated with scaling for continuous motion monitoring system.

- Frequent, noisy, error prone and storage demanding data is expected.

  If sampled at 40HZ with MDAWN, 20 mins of data from 1 tri-axial accelerometer sensor is 1MB. In SIRRACT setting, we assign two sensors to each user, on both ankles. If a user uses the sensor 8 hours a day, the data size will be above 1GB after 1 month. It will be a storage problem if a large population is supported by continuous monitoring.

- Information fusion from multiple sources are needed, such as multiple sensors, previously learned models, context, etc.

- New modeling techniques are required, such as robust estimation and classification framework, advances in machine learning, data mining, modeling and visualization

- Dynamic user models should be hypothesized, since the user's gait might be undergoing changes due to treatment or disease affection.

The performance of scalability can be measured by two metrics: the accuracy of processing and responding time, a.k.a transactions per second. Accuracy should not be sacrificed by the growing amount of processing work. Besides, a reasonable processing time is expected. In order to achieve these two goals, feasible methods include single or combination of the following: added hardware, such as investing more servers, the commercialized service cloud computing, and improved models and algorithms. In this thesis, I concentrate on model and algorithm innovation.

5.2 High Speed Search and Analytics

5.2.1 SPR: An Indexing Algorithm

Data traces from accelerometers and other motion-sensing devices can be compressed by means of symbolic representation, the Significant Point Representation algorithm (SPR). In SPR, only the significant local maximum and local minimum points are identified. In our setting, we normalize the data into range of $[-1\ 1]$ and use a $binwidth = 0.2$, which makes the alphabet size 10, that is, from a to j. This configuration demonstrates good performance in gait characterization; however, the parameter combination can be tuned to other values and fit other applications.

Algorithm 4 shows the procedure of SPR. Data is first normalized to the range of $[-1\ 1]$. Then a convolution-based local maxima and local minima algorithm [loc] is applied. The combination of all the local maxima and local minima are named local significant points. Excessive points will be generated in this step. In order to get the significant points, excessive points have to be removed from local significant points. Significant points satisfy the criterion that the abutted points have a value difference larger or equal to $binwidth$. Algorithm 5 shows the procedure to remove the excessive points according to the input parameter $binwidth$. It iteratively eliminates excessive points in each run (In the implementation, we keep the indices of to-be-deleted points

into an array and subtract this array in the final operation).

Algorithm 4 Significant Point Representation

Input: Input data $x \in R^n$, bin width α

Result: Position of significant points y

25 **begin**

/* normalize data to the range of $[-1\ 1]$ */

26 $x \leftarrow (x - \min(x))/(\max(x) - \min(x)) * 2 - 1$ /* find local maximal and minimal points; excessive points will be generated */

27 $a = local\_max(x, 4)$ /* position of local maxima */

28 $b = local\_min(x, 4)$ /* position of local minima */

29 $localsigp = sort([a\ b])$ /* remove excessive points */

30 $y = \text{remove\_excessive\_p}(\alpha, localsigp, x)$

31 **end**

The position of significant points in gait tend to correspond to different phases of a gait cycle, for instance heel strike or leg swing [Salarian et al., 2004]. This formulation can be validated by the timing analysis of gait phases during a stride in [Saremi et al., 2006].

Figure 5.1 shows the accelerometer trace (blue line) of one axis of an accelerometer that was worn during walking. The data for this trace is normalized to $[-1\ 1]$. The trace includes three strides. The primary axis is oriented vertically, towards the ground. According to [Saremi et al., 2006], the points that are labeled with number 1, 3, 5 are toe-off, which is the start of a swing; the points that are labeled with number 2, 4, 6 are heal-striking, which is the end of a swing. The rest of the stride is the stance phase. As a reference, figure 3.7 shows the graphic illustration of phases in a gait cycle [Cuccurullo, 2004].

The red crosses in Fig 5.1 indicates the derived significant points after SPR algo-

Algorithm 5 Remove Excessive Points

Input: Bin width α, position of local significant points p, input normalized signal $s \in R^n$

Result: Position of significant points y

begin

$\delta s = s(p) - s(p-1)$ $x_1 \leftarrow \forall t, s.t. |\delta s(t)| \leq \alpha$ $x_2 \leftarrow \forall t, s.t. |\delta s(t)| > \alpha$ $p_2 = p(x_2)$

while $\text{length}(x_1) \geq 1$ **do**

$x_r = [\,]$ $c = [\,]$ **for** $n = 1 : \text{length}(x_1) - 1$ **do**

$c = [c; x_1(n)]$ **if** $(x_1(n) - x_1(n+1)) \neq -1$ **then**

$c = [c; c(end) + 1]$ $v = s(p(c))$ $x_k \leftarrow \forall t, s.t. |v(t)| = \max(|v|)$ **if** $\text{length}(x_k) > 1$ **then**

$x_k = x_k(1)$

$x_r = [x_r; c((1 \cdots \text{length}(c)) \setminus x_k)]$ $c = [\,]$ *continue*

if $x_1(n) - x_1(n+1)) \equiv -1$ **then** $c = [c; c(end) + 1]$ **else** $c = [\,]$ $c = [x_1(end); x_1(end) + 1]$ $x_k = \text{find}(|s(p(c))| \equiv \max(|s(p(c))|))$ **if** $\text{length}(x_k) > 1$ **then**

$x_k = x_k(1)$

$x_r = [x_r; c((1 \cdots \text{length}(c)) \setminus x_k)]$ $y = p((1 \cdots \text{length}(p)) \setminus x_r)$ $\delta s = s(y) - s(y-1)$ $x_1 = \text{find}(|\delta s| <= \alpha)$

$y \leftarrow y \cup p_2$

end

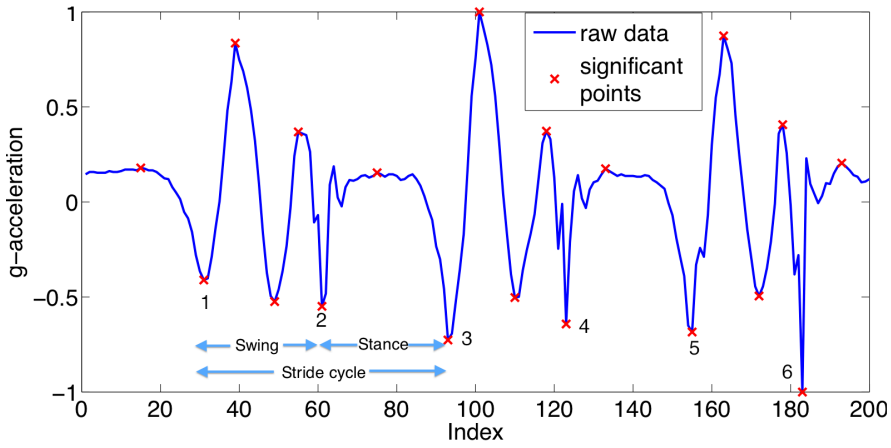

Figure 5.1: An example of SPR

rithm is applied. It can be observed that by labeling the significant points in the trace, stride segmentation occurs naturally and it accords with the validity analysis in [Saremi et al., 2006] as well as the graphic illustration in figure 3.7. The swing phase of gait, when the foot is swinging forwards, corresponds to the longest local minima pair. This swing identification method will be used in the rest of this paper.

5.2.2 Gait Segmentation Evaluation

SPR based gait segmentation can apply to subjects with diverse gait patterns and different motor abilities. SIRRACT study [sir] provides a perfect subject pool to test the performance of the algorithm in gait segmentation.

In SIRRACT, multiple rehabilitation measures are recorded, such as NIH Stroke Scale [nih], functional ambulation category [fac], Barthel Index [O'Sullivan et al., 2004], Stroke Impact Scale [sis], as well as walking speed during trainingXu et al. [2011]. The test subjects are from SIRRACT site 1 and site 2 and 24 subjects are included in total.

We use fac as a reference to cluster subjects with different physical activity abilities. FAC level 0 represents Nonfunctional Ambulation and level 5 represents Ambulator

Independent. The FAC levels provide a full coverage of patients' physical activity ability description. Content of FAC levels is listed below

Description: Staff-completed tick box of 5 broad categories of walking ability Ranges from independent walking outside to non-functional walking Patients can be rated on the following categories:

- 0: Patient cannot walk, or needs help from 2 or more persons
- 1: Patients needs firm continuous support from 1 person who helps carrying weight and with balance
- 2: Patient needs continuous or intermittent support of one person to help with balance and coordination.
- 3: Patient requires verbal supervision or stand-by help from one person without physical contact
- 4: Patient can walk independently on level ground, but requires help on stairs, slopes or uneven surfaces
- 5: Patient can walk independently anywhere

5.2.2.1 Gait Segmentation Examples

Figure 5.2 shows the raw data from patients with different FAC levels and the SPR result on the y-axis. Please note that y-axis is pointing to ground. In each subfigure, the upper plot is from left ankle and the lower plot is from right ankle. When right ankle's data is plotted, the value substracts 8 to avoid plotting overlapping.

From figure 5.2, it can be observed that the segmentation is very effective for patients with FAC level 2 to 5. For patient with FAC 1, the hemiparetic side is not segmented properly due to temporally volatile movement within the stride.

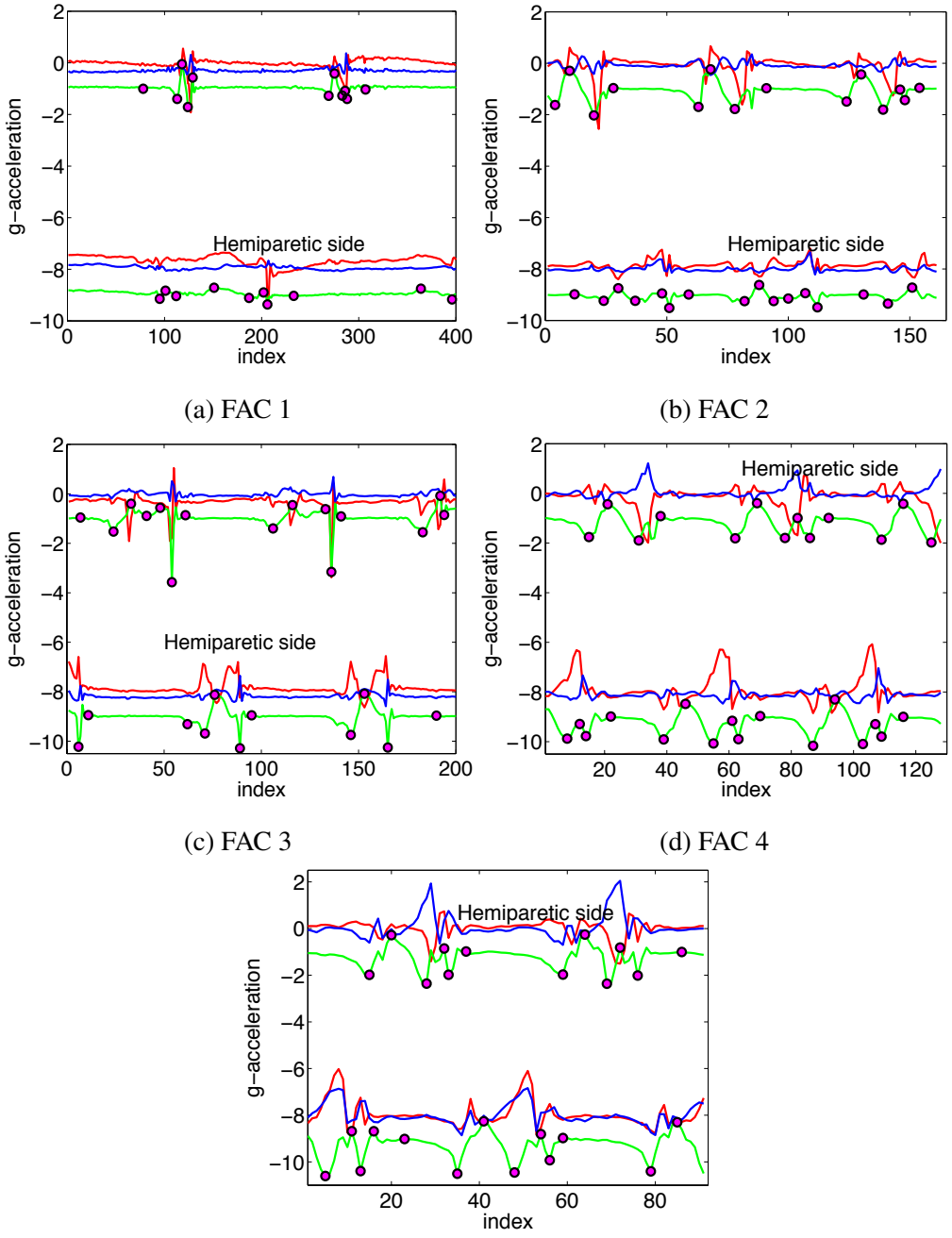

(a) FAC 1

(b) FAC 2

(c) FAC 3

(d) FAC 4

(e) FAC 5

Figure 5.2: Subjects with different FAC levels and the SPR result on y-axis

We use swing detection accuracy as an indicator to assess performance of gait segmentation. This is intuitive, as swing phase is identified, the rest of a stride is stance naturally.

5.2.2.2 Gait Segmentation Performance by SPR

The accuracy of gait segmentation is a layered result since we have two steps in the procedure.

The first layer is peak detection accuracy rate. Over 524 strides, 6 peaks are mislabeled, including 5 false negatives and 1 false positives. The accuracy for peak detection is 98.85%.

The second layer is accuracy rate for SPR and ASM separately. The accuracy of swing detection within one stride is defined in equation 5.1, where s_{GT} and e_{GT} represent ground truth start index and end index of swing within a stride; s and e represent the start index and end index from SPR and ASM algorithm. For an episode of walking, the overall accuracy is arithmetic average of individual accuracies. For subjects within the same FAC level, we take arithmetic average of individuals to get the final accuracy value.

$$accuracy = \frac{\min(e_{GT}, e) - \max(s_{GT}, s)}{\max(e_{GT} - s_{GT}, e - s)} \tag{5.1}$$

The swing detection accuracy rate by SPR and ASM is summarized in table 5.1. It can be observed from talbe 5.1 that SPR outperforms ASM by both accuracy and stability. Here we argue that the misses caused by SPR is due to subjects' inability to make a valid heal striking, that no clear local minima pair were observed within a stride. The misses by ASM is due to the consistency between template and the testing time series. It can be observed that the higher the quality of walking(the more consistent the walking is), the better of the accuracy.

Swing Phase Detection Accuracy											
Methods		FAC level1 (17 strides, 1 subject)		FAC level2 (55 strides, 2 subjects)		FAC level 3 (222 strides, 7 subjects)		FAC level 4 (106 strides, 7 subjects)		FAC level 5 (124 strides, 9 subjects)	
		mean	std	mean	std	mean	std	mean	std	mean	std
SPR	Hemiparetic	0.7968	0.0000	0.7419	0.1339	0.9726	0.0365	0.9674	0.0557	1.0000	0.0000
	Non-hemiparetic	1.0000	0.0000	0.9800	0.0282	0.9428	0.0627	0.9542	0.0570	0.9661	0.0741
ASM	Hemiparetic	0.8029	0.0000	0.7550	0.1524	0.8270	0.1109	0.7937	0.1186	0.8124	0.1134
	Non-hemiparetic	0.8022	0.0000	0.7110	0.1891	0.7829	0.1089	0.8495	0.1178	0.8046	0.1145

Table 5.1: Swing phase detection accuracy summary

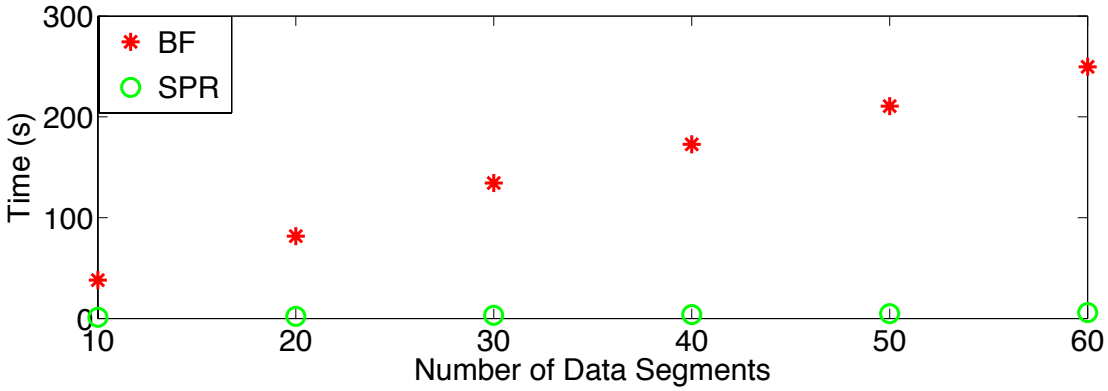

Figure 5.3: Running time comparison between BF and SPR

5.2.3 High Speed Search Example

Running time of swing phase identification using two methods are compared, brute force and SPR. Brute force method is adaptive swing matching. In asm, the algorithm does a point to point distance calculation on raw data directly. In SPR, it operates on top of the significant points. Figure 5.3 shows the running time.

SPR algorithm outperforms asm not only in accuracy but also in running time.

5.3 High Speed Search Principles

Clustering is of my interest after the work of individualized model because of the following reasons. First, we have data archived from diverse subjects by SIRRACT study. It will be interesting to explore and summarize the diversity of gait in the database, which sets the basis of scaling for large populations. Second, manual inspection and

expert input for classification are inevitable. In SIRRACT study, the subject might walk independently for training and then use assistive device for testing, which makes the feature distribution in training deviates from the testing data. Besides, certain activities can have same statistical feature distribution as the target motion and confuses classifier(for example in figure 3.21 a). For the sake of accuracy in classification and outcome measures, manual inspection is needed. Third, clustering is an unsupervised learning method. It saves the work for inconvenient supervised learning modality. In SIRRACT study, training is required on a weekly basis, which is tedious and error prone.

In order to fulfil the above objectives, I have the following hypotheses

1. A finite number of gait patterns, the primitive patterns, exist in humans.

2. The SIRRACT database is representative to derive the primitive patterns.

The benefits foreseen from the clustering includes improving the classification accuracy and exploration of correlation between primitive gait patterns and diseases.

5.3.1 Gait Pattern

The gait pattern is defined as the temporal envelope of a stride signal recurring in many other subjects gait data. Gait pattern has two types of variances, the amplitude variance and local warping variance. Amplitude variance means the amplitude of gait from the same gait pattern can have varied signal strength. Local warping variance means the time spent in different phases of the gait may vary for gaits in the same pattern.

Figure 5.6 shows 6 plots of individual gait from different subjects. Intuitively, gait 1 to 4 belong to the same cluster, since they all have the 6-point repetitive pattern in gait, though variance exists in speed and amplitude. Gait 5 and gait 6 belong to separate clusters, since their temporal spread is distinct from others.

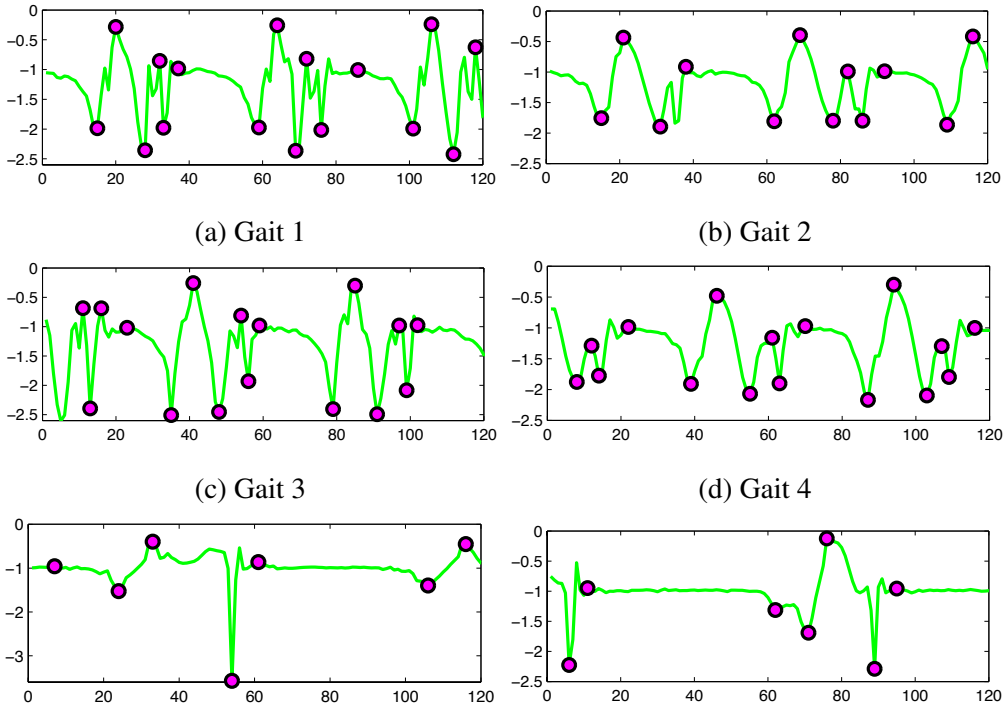

(a) Gait 1 (b) Gait 2

(c) Gait 3 (d) Gait 4

(e) Gait 5 (f) Gait 6

Figure 5.4: Gait pattern examples

The 6-point repetitive pattern starts from toe-off, spreads on entire swing phase and ends on the start or middle of stance. Most gait in population follow this pattern, as shown in section 5.3.2.3

5.3.2 Hierarchical Clustering

5.3.2.1 Clustering Introduction

In supervised learning, labeled training data is provided to learn the description of classes, or feature distribution in our case, as discussed in section 3.3. This feature distribution then will be applied to label new testing data. In clustering, however, the task is to group unlabeled data into meaningful clusters so that data from the same cluster are more similar compared with data from different clusters. It is an explorative

method since usually no prior knowledge is available and least assumption should be made about the data.

The widely applied clustering method include hierarchical clustering, mixture model and K-means, and k-means is a simplified version of mixture model. The problem with mixture model and k-means methods are they are sensitive to initialization. Take k-means as an example, the final clustering result depends on the initial assignment of cluster centers and cluster number. Besides, hierarchical clustering is more flexible, since the dendrogram generated by hierarchical clustering can be broken at different levels to generate different number of clusters. Thus hierarchical clustering method is explored, particularly bottom up, agglomerative hierarchical clustering is employed in the thesis.

In agglomerative hierarchical clustering, each single point is a cluster of its own. Next most similar clusters are merged as a parent cluster. This is repeated until the complete dataset has been merged into one cluster.

5.3.2.2 Similarity Measurement

In hierarchical clustering, it is the basis to first generate a distance matrix among data. The most famous similarity measurement metric is euclidean distance defined as

$$d(x_i, x_j) = (\sum_{k=1}^{d}(x_{i,k} - x_{j,k})^2)^{1/2} = ||\mathbf{x}_i - \mathbf{x}_j||_2 \tag{5.2}$$

However, the conventional euclidean distance will not accommodate amplitude variance and local warping variance, as required in section 5.3.1. A local warping variance example is shown in figure 3.6. Instead, I use the returned distance metric from dynamic time warping algorithm, which sums up the euclidean distance along the warping path.

Given the data segment which includes many strides from the same subject, SPR is first applied to derive an abbreviated representation of data. The task then is to first find the recurring stride from the subject. The recurring stride is called instance in

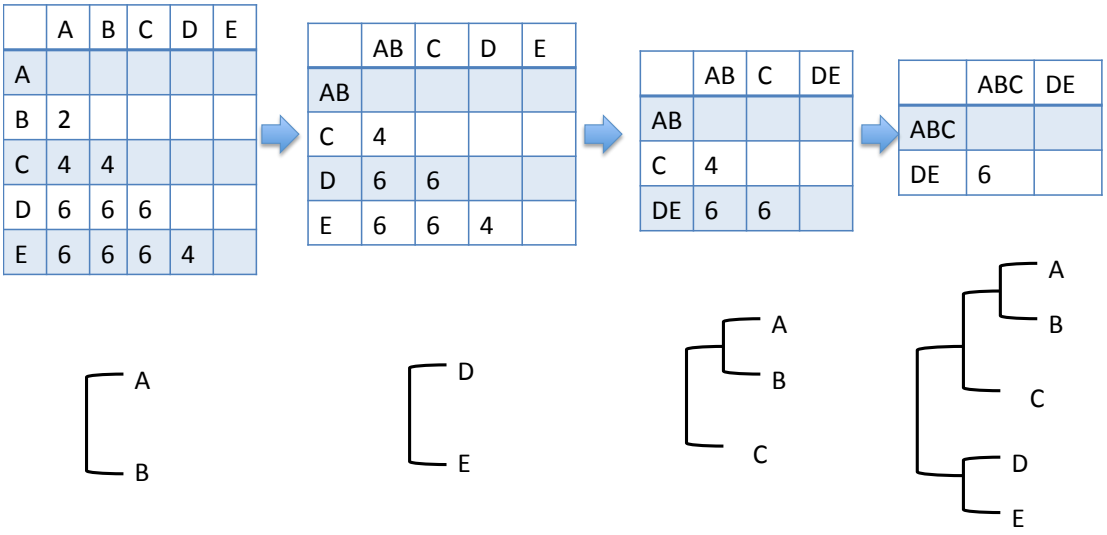

Figure 5.5: UPGMA based dendrogram generation

this thesis. Peculiar strides will be removed using the entropy method in section 4.2.2, where I keep the cluster with the most strides and choose the first stride from that cluster as instance for this subject.

After instances from all the subject are derived, a dtw based distance matrix is generated among the instances. It is referred as the similarity matrix.

5.3.2.3 Dendrogram

Given the similarity matrix, the dendrogram is built up. I use UPGMA (unweighted pair group method with arithmatic mean) to calculate distance between clusters. In UPGMA, distance between clusters is defined as the arithmatic average of the sub clusters. Figure 5.5 shows an example of how to construct a dendrogram based on a similarity matrix. The distance between cluster A,B and C is defined as $(distance(A, C) + distance(B, C))/2$.

The data pool includes 371 data segments of gait, with an averaged length of 50 seconds. Wherein 351 data segments are from SIRRACT database and the rest 20 are

from healthy subjects with normal gait. The 351 data segments are derived in a way that I sampled all patients data every 7 days.

As discussed before, one instance will be abstracted from a data segment and 371 instances will be generated in this case. ID 1 to 20 are from normal subjects and 21 to 371 are from patients. Those instances may or may not follow the same primitive gait pattern.

Different dendrograms are generated by different number of instances to validate the stability of the dendrogram structure. Figure 5.6 a to g shows the dendrogram structures trend by varying the number of instances and no major fluctuations are observed.

Note that figure 5.6 g is the generated dendrogram from all instances. By breaking the dendrogram at different levels, different number of clusters will be generated. This is very convenient since the resolution of clustering is under control.

By breaking the dendrogram in figure 5.6 at a distance 20, 12 clusters are generated shown in figure 5.7. Different number of instances are under each cluster and they are summarized below:

- Cluster 9: 1 instance
- Cluster 10: 2 instances
- Cluster 1: 344 instances
- Cluster 2: 7 instances
- Cluster 3: 5 instances
- Cluster 8: 4 instances
- Cluster 6: 3 instances
- Cluster 11: 1 instance

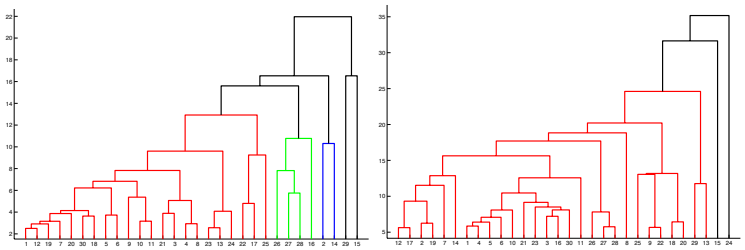

(a) 50 (b) 100

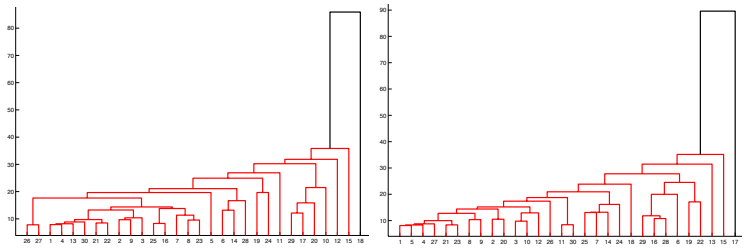

(c) 150 (d) 200

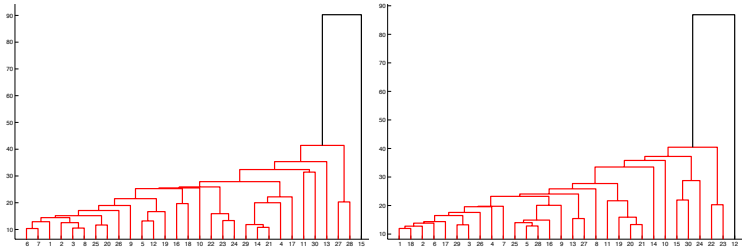

(e) 250 (f) 300

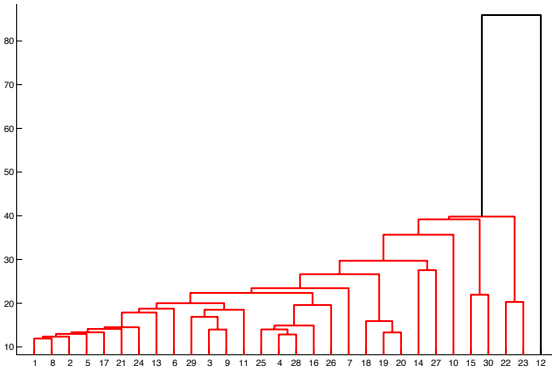

(g) 371

Figure 5.6: Gait pattern examples

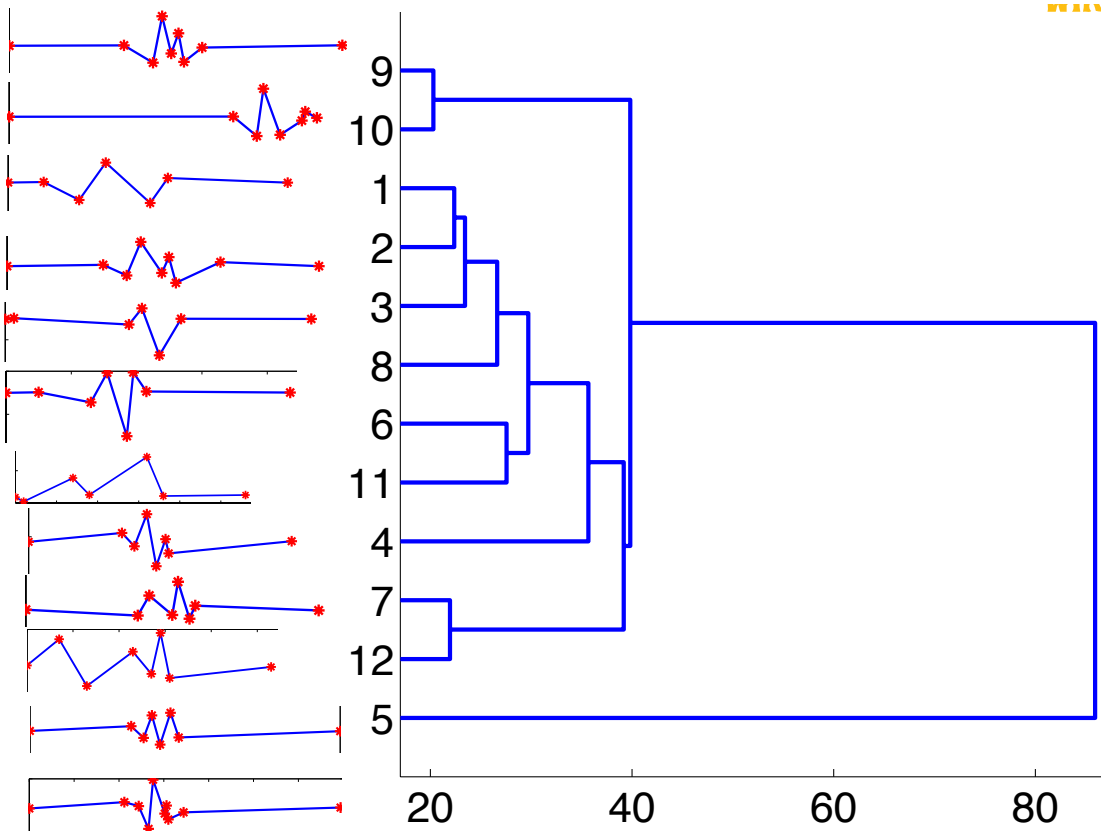

Figure 5.7: Twelve primitive gait patterns

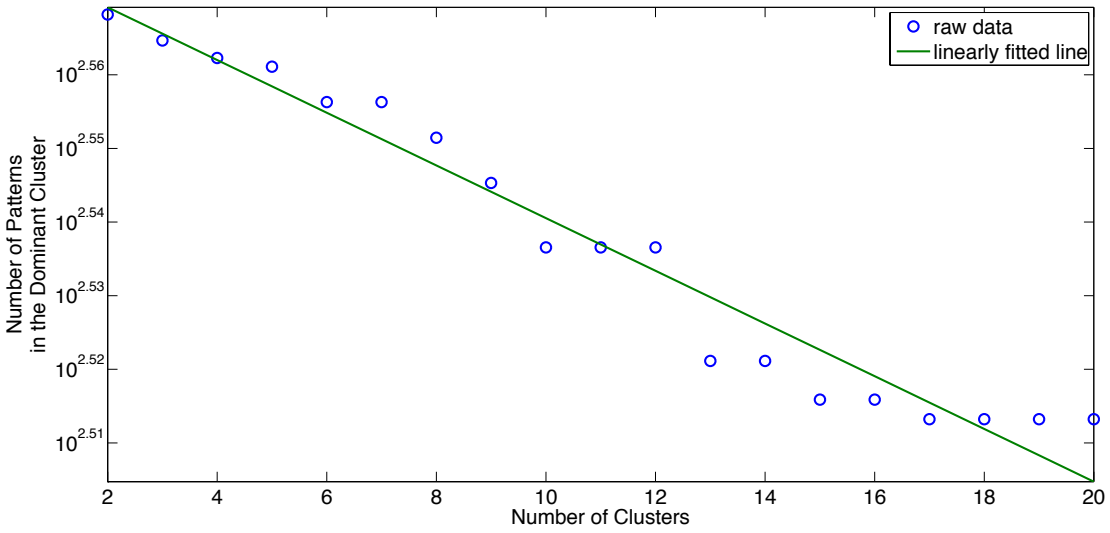

Figure 5.8: The scaling of gait patterns per dominant cluster

- Cluster 4: 1 instance
- Cluster 7: 1 instance
- Cluster 12: 1 instance
- Cluster 5: 1 instance

In each cluster, a representative gait pattern, which is recurring in instances under that cluster, is shown in the left side of figure 5.7. They are the derived primitive gait patterns referred in section 5.3.1. Particularly majority of instances are under cluster 1. The primitive gait pattern in cluster 1 is the widely observed 6-point pattern that starts from toe off, spreads through the complete swing and ends at the start or middle of instance. Please note the primitive gait pattern is repetitive and thus cyclic in data segments. The primitive gait pattern shown under cluster 1 is 5 points shifted.

A log-linear relationship is found between number of instances and the number of clusters. That is, by breaking the dendrogram at different levels, the number of instances within the dominant cluster will grow exponentially. It supports scaling for

big data, since the majority of the population will follow a validated gait pattern, and manual inspection and expert input will be only needed for the rarely presented cases. A refined gait pattern library can be gradually built up with increased size of population.

5.4 Discussion

In this chapter, I introduce the developed techniques of scaling the current system to support a large population. Particularly, SPR, an indexing method that is specialized in motion analysis is brought up. It enables data dimension reduction with least information loss as well as automated gait segmentation. Primitive gait patterns from the stroke population are derived, which is informative to stroke subject motion pathology. Scaling to a large population is enabled by SPR and a refined primitive gait pattern library.

CHAPTER 6

Conclusion and Future Work

6.1 Dissertation Conclusion

Previous chapters of this thesis explore the means of motion sensing used as monitoring, from constrained exercise to ambulatory daily activity, from individualized model to population based analysis. Accelerometer based motion sensing is employed due to the concern of battery life.

This thesis first presents StepFit: a fitness evaluation system using wearable sensors. It is an automated self-administered, low cost and convenient system for fitness evaluation, heart rate response analysis and prediction The motion sensing is in charge of monitoring exercise intensity (step frequency). StepFit involves stepping, which is a constrained and highly repetitive exercise and the system has minimum workload intensity requirement, even if different subjects perform the exercise, the individual difference will not affect the motion sensing part and thus the monitoring itself is easy to achieve.

It then steps into the area of ambulatory activity monitoring for patients. Gait is of particular interest. The signal from patients are generally irregular, non-consistent and weak and it poses challenge in both classification and kinematic characterization. We introduce hybrid classification and adaptive peak detection to leverage this problem. Besides, the gait data presents diversity among subjects, wherein individualized classification model is desirable. We further introduce the technical details of the inter-

national trial, the SIRRACT study. I also summarize the encountered problems in large scale trial and the engineering solutions. During SIRRACT, longitudinal data through continuous monitoring is archived. A method that visualizes patient's gait evoluation longitudinally is introduced. By comparing with a control group composed of normal gaits, it provides a macroscopical and direct view of visualizing patient's recovery path.

As the subject's number in SIRRACT as well as diversity increase, the individualized model cannot fully exhibit and utilize the recurring diversity type that has been observed and processed. Besides, for a large population, the individualized model needs complex user training thus hard to be adopted by large community and it's expensive in term of computing resources. Motivated by the above reasons, I first introduce SPR, an indexing algorithm that will abbreviate data with reduced dimension and minimal information loss. Further, I utilize hierarchical clustering to generate the recurring gait patterns, referred as primitive gait patterns. This is informative for stroke community. With gait data from different resources , a refined primitive gait library will be built up to represent a large population.

6.2 Future Work

Based on the current research presented in this thesis, there are still many opportunities not yet be investigated. In the following, we provide a short outline of future lines of work which is built on the results of the present thesis.

1. Validate the classification result with the generated primitive gait patterns on SIRRACT and compare the performance with the method introduced in chapter 3.

2. Clean up and build an anonymous database of diverse subjects' data, which includes raw data, classification, kinematic parameters, gait segmentation, the belonged gait pattern and rehabilitation evaluation. The database will be hosted by UCLA Wireless Health Institute website and works as a featured benchmark for

other researchers to validate their algorithms.

3. Extend the work of longitudinal analysis of SIRRACT study in chapter 4. First, develop a scoring system that combines both kinematic parameters from motion sensing and rehabilitation scale by physician evaluation. Second, incorporate all the patients in SIRRACT into the longitudinal analysis.

4. Explore the possibility of using single sensor for classification, kinematic characterization and energy expenditure calculation. It will facilitate community adoption and open the possibility of large population usage.

5. Explore motion sensing and general time series analysis in other areas of health monitoring, such as motion monitoring for hip replacement surgery complications, digestive monitoring with acoustic sensors, etc. Validate the scaling rationale introduced in chapter 5 in those areas.

BIBLIOGRAPHY

Gaitrite. Website. http://www.gaitrite.com/.

Metamotiongypsy. Website. http://www.metamotion.com/gypsy/gypsy-motion-capture-system.htm.

Optitrack. Website. http://www.naturalpoint.com/optitrack/.

Polhemus. Website. http://www.polhemus.com/.

Shapewrap. Website. http://www.motion-capture-system.com/.

Vicon. Website. http://www.vicon.com/.

Rehab measures: Functional ambulation category. Website. http://www.rehabmeasures.org/Lists/RehabMeasures/DispForm.aspx?ID=920.

Local minimum. Website. http://www.mathworks.com/matlabcentral/fileexchange/3170-local-min-max-nearest-neighbour.

Mdawn. Website. http://www.gcdataconcepts.com/index.html.

Motionstart. Website. http://ascension-tech.com/.

Nih stroke scale. Website. http://www.nihstrokescale.org/.

Polar heart rate module - rmcm01. Website. http://www.sparkfun.com/products/8660.

Polar transmitters and straps. Website. http://www.heartratemonitorsusa.com/polar-straps.html?gclid=CLyqjPbnyacCFQM6gwodvjo3Dg.

Sirractpilot. Website. http://eawins38.ee.ucla.edu/~whi_process/sirract/.

Rehab measures: Stroke impact scale. Website. http://www.rehabmeasures.org/Lists/RehabMeasures/DispForm.aspx?ID=934.

Stroke scale overview. Website. http://www.strokecenter.org/trials/scales/scales-overview.htm.

J. K. Aggarwal and M. S. Ryoo. Human activity analysis: A review. *ACM Computing Surveys*, 43:16:1–16:43, 2011.

A. H. Association. Stroke statistics: Us statistics. Website. http://www.strokecenter.org/patients/about-stroke/stroke-statistics/.

L. Au, W. Wu, M. Batalin, D. Mclntire, and W. Kaiser. MicroLEAP: Energy-aware Wireless Sensor Platform for Biomedical Sensing Applications. In *Biomedical Circuits and Systems Conference*, pages 158 –162, 2007.

L. Bao and S. S. Intille. Activity recognition from user-annotated acceleration data. *Lecture Notes in Computer Science*, 3001, 2004.

C. M. Bishop. *Pattern Recognition and Machine Learning*. Springer, 2006.

C. Bouten, K. Koekkoek, M. Verduin, R. Kodde, and J. Janssen. A triaxial accelerometer and portable data processing unit for the assessment of daily physical activity. *IEEE Transactions on Biomedical Engineering*, 44(3):136–147, 1997.

L. Brouha, C. Health, and A. Graybiel. Step test simple method of measuring physical fitness for hard muscular work in adult men. *Review of Canadian Biology*, 2:86–92, 1943.

C. Cole, J. Foody, E. Blackstone, and M. Lauer. Heart rate recovery after submaximal exercise testing as a predictor of mortality in a cardiovascularly healthy cohort. *Annals Internal Medicine*, 132(7):552–555, 2000.

S. J. Cuccurullo. *Physical Medicine and Rehabilitation Board Review*. New York: Demos Medical Publishing, 2004.

H. Cullumbine, S. W. Bibile, and T. W. Wikramanayake. Influence of age, sex, physique and muscular development on physical fitness. *Journal of Applied Physiology*, 2(9): 488–511, 1950.

B. Dobkin, S. Thomas, X. Xu, M. Batalin, and W. Kaiser. Reliability of bilateral ankle accelerometer algorithms for activity pattern recognition and walking speed after stroke. *Stroke*, 42(8):2246–2250, 2011a.

B. H. Dobkin, X. Xu, M. Batalin, S. Thomas, and W. Kaiser. Reliability and validity of bilateral ankle accelerometer algorithms for activity recognition and walking speed after stroke. *Stroke*, 42:2246–2250, 2011b.

J. Dougherty, R. Kohavi, and M. Sahami. Supervised and Unsupervised Discretization of Continuous Features. In *12th International Conference on Machine Learning*, pages 194–202, 1995.

K. R. Fox. The influence of physical activity on mental well-being. *Public Health Nutrition*, 2:411–418, 1999.

H. Ghasemzadeh, V. Loseu, and R. Jafari. Collaborative signal processing for action recognition in body sensor networks: A distributed classification algorithm using motion transcripts. In *The 9th ACM/IEEE International Conference on Information Processing in Sensor Networks*, 2010.

P. T. Gibbs and H. H. Asada. Wearable conductive fiber sensors for multi-axis human joint angle measurements. *Journal of NeuroEngineering and Rehabilitation*, 2(1):7, 2005.

J. Gower and G. Dijksterhuis. *Procrustes Problems*. Oxford University Press, 2004.

Y. Hong, J. X. Li, and P. D. Robinson. Balance control, flexibility, and cardiorespiratory fitness among older tai chi practitioners. *British Journal of Sports Medicine*, 34(1): 29–34, 2000.

R. E. Johnson, L. Brouha, and R. C. Darling. A test of physical fitness for strenuous exertion. *Revue Canadienne de Biologie*, 1:491–503, 1942.

J. Liu, L. Zhong, J. Wickramasuriya, and V. Vasudevan. uwave: Accelerometer-based personalized gesture recognition and its applications. In *IEEE International Conference on Pervasive Computing and Communications*, 2009.

A. Lopez-S., R. Vial, L. Balart, and G. Arroyave. Effect of exercise and physical fitness on serum lipids and lipoproteins. *Atherosclerosis*, 20:1–9, 1974.

M. J. Mathie, B. G. Celler, N. H. Lovell, and A. C. Coster. Classification of basic daily movements using a triaxial accelerometer. *Medical & biological engineering & computing*, 42(5):679–687, 2004.

U. Maurer, A. Smailagic, D. P. Siewiorek, and M. Deisher. Activity recognition and monitoring using multiple sensors on different body positions. In *Proceedings of the International Workshop on Wearable and Implantable Body Sensor Networks*, 2006.

W. D. McArdle, F. I. Katch, G. S. Pechar, L. Jacobson, and S. Ruck. Reliability and interrelationships between maximal oxygen intake, physical work capacity and step-test scores in college women. *Medicine and Science in Sports and Exercise*, 4:182–186, 1972.

R. E. D. Meersman. Heart rate variability and aerobic fitness. *American Heart Journal*, 125:726–731, 1993.

J. Mizuo, T. Nakatsu, T. Murakami, S. Kusachi, Y. Tominaga, K. Mashima, T. Uesugi, H. Ueda, C. Suezawa, and T. Tsuji. Exponential Hyperbolic Sine Function Fitting of

Heart Rate Response to Constant Load Exercise. *The Japanese Journal of Physiology*, 50:405–412, 2000.

O. Oken, G. Yavuzer, S. Ergöçen, Z. R. Yorgancoglu, and H. J. Stam. Repeatability and variation of quantitative gait data in subgroups of patients with stroke. *Gait Posture*, 27(3):506–11, 2008.

O'Sullivan, S. B, and T. J. Schmitz. *Physical Rehabilitation, Fifth Edition*. F.A. Davis Company, 2004.

K. K. Patterson, W. H. Gage, D. Brooks, S. E. Black, and W. E. McIlroy. Changes in gait symmetry and velocity after stroke: a cross-sectional study from weeks to years after stroke. *Neurorehabilitation and Neural Repair*, 24(9):783–90, 2010.

W. H. Press and B. P. Flannery. *Numerical Recipes in C: The Art of Scientific Computing*, chapter 15.5. Cambridge University Press, 1988.

N. B. Priyantha, A. Chakraborty, and H. Balakrishnan. The cricket location-support system. In *Proceedings of the Sixth Annual ACM International Conference on Mobile Computing and Networking*, pages 32–43, 2000.

D. Roetenberg, P. J. Slycke, and P. H. Veltink. Ambulatory position and orientation tracking fusing magnetic and inertial sensing. *IEEE Transactions on Biomedical Engineering*, 54(5):883–890, 2007.

D. Roetenberg, H. Luinge, and P. Slycke. Xsens mvn : Full 6dof human motion tracking using miniature inertial sensors. Technical report, Xsens Motion Technologies, 2009.

I. Ryhming. A modified harvard step test for the evaluation of physical fitness. *Arbeitsphysiologie*, 15(3):235–250, 1954.

H. Sakoe and S. Chiba. Dynamic programming algorithm optimization for spoken

word recognition. *IEEE Transactions on Acoustics, Speech and Signal Processing*, 26:43–49, 1978.

H. Sakoe and S. Chiba. Readings in speech recognition. chapter Dynamic programming algorithm optimization for spoken word recognition, pages 159–165. Morgan Kaufmann Publishers Inc., San Francisco, CA, USA, 1990.

A. Salarian, H. Russmann, F. J. G. Vingerhoets, C. Dehollain, Y. Blanc, P. R. Burkhard, and K. Aminian. Gait assessment in parkinson's disease: Toward an ambulatory system for long-term monitoring. *IEEE Transactions on Biomedical Engineering*, 51(8):1434–43, 2004.

K. Saremi, J. Marehbian, X. Yan, J.-P. Regnaux, R. Elashoff, B. Bussel, and B. H. Dobkin. Reliability and validity of bilateral thigh and foot accelerometry measures of walking in healthy and hemiparetic subjects. *Neurorehabil Neural Repair*, 20(2): 297–305, 2006.

H. M. Schepers and P. H. Veltink. Stochastic magnetic measurement model for relative position and orientation estimation. *Measurement Science and Technology*, 21(6): 065801, 2010.

R. J. Shephard. The relative merits of the step test, bicycle ergometer, and treadmill in the assessment of cardio-respiratory fitness. *Internationale Zeitschrift für Angewandte Physiologie, Einschliesslich Arbeitsphysiologie*, 23(3):219–230, 1966.

L. S. Stephenson, M. C. Latham, S. N. Kinoti, K. M. Kurz, and H. Brigham. Improvements in physical fitness of kenyan schoolboys infected with hookworm, trichuris trichiura and ascaris lumbricoides following a single dose of albendazole. *Transactions of the Royal Society of Tropical Medicine and Hygiene*, 84:277–282, 1990.

M. Supej. 3d measurements of alpine skiing with an inertial sensor motion capture suit and gnss rtk system. *Journal of Sports Sciences*, 28:759 – 769, 2010.

D. Vlasic, R. Adelsberger, G. Vannucci, J. Barnwell, M. Gross, W. Matusik, and J. Popovic. Practical motion capture in everyday surroundings. *ACM Transactions on Graphics*, 26(3):35:1–35:9, 2007.

Y. Wang, X. Xu, M. Batalin, and W. Kaiser. Detection of upper limb activities using multimode sensor fusion. In *IEEE Biomedical Circuits and System Conference*, pages 436–439, 2011.

D. E. Warburton, C. W. Nicol, and S. S. Bredin. Health benefits of physical activity: the evidence. *Canadian Medical Association Journal*, 174(6):801–809, 2006.

X. Xu, M. A. Batalin, W. J. Kaiser, and B. Dobkin. Robust hierarchical system for classification of complex human mobility characteristics in the presence of neurological disorders. In *International Workshop on wearable and Implantable Body Sensor Networks*, volume 0, pages 65–70, 2011.